Time-Dependent Compressibility of Poly (Methyl Methacrylate) (PMMA): An Experimental and Molecular Dynamics Investigation

Thesis by

Sandeep Sane

In Partial Fulfillment of the Requirements
for the Degree of
Doctor of Philosophy

Graduate Aeronautical Laboratories
California Institute of Technology
Pasadena, California

2001

(Defended July 6, 2000)

This thesis is dedicated to my parents,
my sister and Atul.

Acknowledgements

First and foremost, I would like to express my sincere thanks to Professor W.G. Knauss for his guidance, support and encouragement during the entire course of this study. His patience and confidence in me have been a great source of motivation and support throughout my graduate studies. Working with him over the last four years, I have learned many valuable lessons, which will continue to guide me throughout my career.

Next, I would like to express my gratitude to Dr. T. Cagin for guiding me through the molecular dynamics simulations and helping me understand the subject by answering my numerous questions patiently. I always enjoyed the candid discussions we had on various topics.

I would like to thank Professor G. Ravichandran, who was also my academic advisor during my first year at Caltech, for chairing my thesis committee. Also I would like to thank Professors K. Bhattacharya and M. Ortiz for taking time to review my thesis.

I also wish to thank many staff members who provided assistance and kindness during this time. Special thanks to Petros Arakelian, who was always helpful and resourceful, Ali Kiani for all the basic lessons in the machine shop, and Alan Goudy for all the assistance in dealing with various electronic instruments.

One of the best things at Caltech has been my fellow graduate students who added an extra dimension to my life other than Mechanics during my stay here. I am grateful to all of them for making all these years very pleasant and enjoyable. First of all, I would like to thank all my group mates, Dr. Sairam Sundaram, Ioannis Chasiotis, Ying Huang, Weidong Zhu and Luis Gonzalez. Special thanks to my office mates, Pradeep Guduru, Omprakash Samudrala and Demirkan Coker for providing immeasurable assistance and

suggestions through out my stay at Caltech and for all the lively discussions we had for hours on a wide variety of topics usually accompanied by the late night donut trips. I wish to thank my "Lunch buddies" – Eric Burcsu and Lavi Zuhal for the countless hours of discussion about Pune and their interest in the "Punenian things". Special thanks to my "Red Door friends" – Dr. Goutam Chattopadhyay and Sujoy Mukhopadhyay, who showed up for coffee at 3.00pm almost everyday in regards to a long standing tradition started in my first year at Caltech. I also wish to thank Nitin Deshpande, Ravinder Abrol, Amit Manwani, Prashant Purohit and Sulekha Chattopadhyay, for their friendship over the years, the memories of which I will continue to cherish. It is difficult to do justice in this brief space to all the people I owe thanks to and I apologize for not mentioning all of them by name.

The present work was funded by the National Science Foundation. This financial support is gratefully acknowledged.

Last but not the least, I would like to thank the most influential people in my life, my parents, my sister, Suvarna, and Atul, for their love and encouragement which has led me to this endeavor. I am indebted to my parents for their unwavering belief in education and for all the sacrifices they made for my education. To them I dedicate this work.

Abstract

This thesis contains three chapters, which describe different aspects of an investigation of the bulk response of Poly(Methyl Methacrylate) (PMMA). The first chapter describes the physical measurements by means of a Belcher/McKinney-type apparatus. Used earlier for the measurement of the bulk response of Poly(Vinyl Acetate), it was now adapted for making measurements at higher temperatures commensurate with the glass transition temperature of PMMA. The dynamic bulk compliance of PMMA was measured at atmospheric pressure over a wide range of temperatures and frequencies, from which the master curves for the bulk compliance were generated by means of the time-temperature superposition principle. It was found that the extent of the transition ranges for the bulk and shear response were comparable. Comparison of the shift factors for bulk and shear responses supports the idea that different molecular mechanisms contribute to shear and bulk deformations.

The second chapter delineates molecular dynamics computations for the bulk response for a range of pressures and temperatures. The model(s) consisted of 2256 atoms formed into three polymer chains with fifty monomer units per chain per unit cell. The time scales accessed were limited to tens of pico seconds. It was found that, in addition to the typical energy minimization and temperature annealing cycles for establishing equilibrium models, it is advantageous to subject the model samples to a cycle of relatively large pressures (GPa-range) for improving the equilibrium state. On comparing the computations with the experimentally determined "glassy" behavior, one finds that, although the computations were limited to small samples in a physical sense, the primary limitation rests in the very short times (pico seconds). The molecular dynamics

computations do not model the physically observed temperature sensitivity of PMMA, even if one employs a hypothetical time-temperature shift to account for the large difference in time scales between experiment and computation. The values computed by the molecular dynamics method do agree with the values measured at the coldest temperature and at the highest frequency of one kiloHertz.

The third chapter draws on measurements of uniaxial, shear and Poisson response conducted previously in our laboratory. With the availability of four time or frequency-dependent material functions for the same material, the process of interconversion between different material functions was investigated. Computed material functions were evaluated against the direct experimental measurements and the limitations imposed on successful interconversion due to the experimental errors in the underlying physical data were explored. Differences were observed that are larger than the experimental errors would suggest.

Contents

List of Figures

List of Tables

Introductory Remarks

For the full description of isotropic material in the linear theory of viscoelasticity, only two material functions are needed, in principle. One of these describes the time-dependence of the shear behavior (or uniaxial behavior), the other the bulk (volumetric) response (or Poisson's response). The shear and uniaxial response of polymers in relaxation or creep have been measured extensively, if not routinely, in the past. However, disproportionately little attention has been given to measuring the bulk (volumetric) response of these materials. To date, the time or rate-dependent bulk response of a polymer over a significant time or frequency range has been determined essentially in only two investigations (McKinney and Belcher, 1963; Deng and Knauss, 1997).[1] The primary reason for the disparity in the number of measurements of shear or uniaxial response on the one hand, and bulk behavior on the other, are the difficulties associated with the experimental methods available for measuring the bulk response of polymers. To accomplish this goal, one needs to access exceedingly small volume variations with a high degree of accuracy. The classical measurements on PVAc by McKinney and Belcher in the 1963 (McKinney and Belcher, 1963) established that the viscoelastic bulk response changes by a relatively small factor of two to four through the transition range when compared to a factor of one hundred to a thousand for the shear or uniaxial behavior. Therefore, the assumptions of constant bulk modulus or compliance did not pose serious impedance in applications of linearly viscoelastic theory to engineering problems.

[1] Both studied were carried out on Poly (vinyl acetate) (PVAc).

However, in the context of non-linearly viscoelastic behavior of polymers, it has been demonstrated in recent studies that dilatation (volume changes) plays a crucial role on the time-dependent mechanical behaviors. Once the small deformation range is exceeded (above 0.2% strain level), even a small volume change induced through mechanical straining can account for highly nonlinear material response such as yield-like behavior, by coupling shear and volumetric responses. Knauss and Emri (1981, 1987) and Losi and Knauss (1992) have elaborated on the mutual dependence of the shear and bulk response through their formalism of constitutive models based on the free volume theory. Duran and McKenna (1990) and Lu and Knauss (1997) further supported this interdependency between the dilatational and shear deformations through experimental observations. It is clearly of interest for better understanding the non-linear response of polymers, that more careful characterization of time-dependent bulk response is needed.

The bulk response of Poly (methyl methacrylate) (PMMA) was determined experimentally and these measurements were compared with molecular dynamics simulations. The experimental method used was based on the Belcher/McKinney method (McKinney *et al.*, 1956). Measurements were carried out by confining a polymer sample in a small cavity under controlled pressures and by applying small cyclic pressure variations by means of a piezoelectric transducer. An experimental apparatus along with relevant electronic circuitry developed by Deng and Knauss (1997), in connection with their work on PVAc, served as the basic equipment for the measurements. To accommodate the higher temperature requirements of PMMA, the apparatus had to be modified. Measurements were carried out over a wide range of temperatures and frequencies. Chapter I summarizes this investigation.

Molecular dynamics simulations were performed to compute the bulk compliance of PMMA as a function of temperature. Molecular models of amorphous PMMA were built and NPT dynamics, i.e., constant number of particles, pressure and temperature, were performed. The results from the computations were compared with the corresponding values of laboratory measurements to assess the efficacy of the numerical method. This effort is delineated in Chapter II.

The third Chapter is devoted to an additional exploitation of the bulk measurements in Chapter I. Within the realm of linear viscoelasticity for any isotropic material, only two independent material functions need to be measured, from which all others can be computed unequivocally, whether in the typical time or frequency domains, using simple analytical expressions. For the first time experimental data on all the four material functions on the same material, PMMA, have become available over a relatively large, if not complete, time or frequency range. Various material functions of PMMA were measured, namely, the relaxation moduli in uniaxial tension, $E(t)$, and in shear, $\mu(t)$, as well as Poisson's ratio, $\nu(t)$, (Lu *et al.*, 1997) and the dynamic bulk compliance, $M^*(\omega)$, from the present study. With the availability of all the four time or frequency-dependent material functions on the same material, the process of interconversion between different material functions was investigated. The computed material functions were evaluated with the direct experimental measurements, and the limitations imposed on successful interconversion due to the experimental errors in the underlying physical data were explored.

Chapter 1

The Time-Dependent Bulk Response of Poly (Methyl Methacrylate) (PMMA)

1.1 Abstract

The dynamic bulk compliance of Poly (Methyl Methacrylate) (PMMA) has been determined at atmospheric pressure over a wide range of temperatures and frequencies, following a new examination of the bulk response of Poly (Vinyl Acetate) (PVAc) at different pressures. While the overall bulk behavior of the current measurements of PVAc agrees fairly well with those reported by Deng and Knauss (1997) at atmospheric pressure, a discrepancy in primarily the frequency response of the storage compliance is accredited to a difference in the moisture contents of the specimens. In PMMA, strong evidence of effects of physical aging on the volumetric behavior is observed and a careful prescription of thermal history was thus necessary to obtain consistent results. The master curves for the bulk compliance are generated by means of the time-temperature superposition principle. A comparison of the bulk and shear response shows that the extent of the transition ranges for the two material functions are comparable. Further comparison of the shift factors for bulk and shear responses supports the idea that different molecular mechanisms contribute to shear and bulk deformations. Another key observation regards the time-temperature superposition principle when applied to bulk compliance data of PMMA. The shifting procedure appears to lead to consistent results for temperatures below 92 °C; however, its validity may have to be questioned for higher

temperatures. This failure is tentatively attributed to the presence of primary (α) and secondary (β) relaxation mechanisms with the latter possibly playing a dominant role in controlling the bulk deformations in the higher temperature range.

1.2 Introduction

The use of polymers as engineering materials has increased remarkably in recent years and it will continue to grow rapidly. To achieve reliable engineering structures and designs, it is essential to characterize the time and temperature dependent material functions of polymers. Within the context of linearly viscoelastic behavior, it is sufficient for any analysis effort to define any two of the four material functions (in relaxation or creep) describing uniaxial, shear, bulk or Poisson response. In principle, none of these responses is fundamentally more important than any other. However, it is well known that in the small deformation range any arbitrary stress or strain state can be expressed in terms of volumetric or dilatational and deviatoric or shear components. The bulk and shear material functions provide, therefore, a complete constitutive description for the material. Numerous researchers have measured the shear response of many polymer systems over the last few decades. However, disproportionately little attention has been given to measuring the bulk (volumetric) response of these systems. To date, the time or rate-dependent bulk response of a polymer over a significant time or frequency range has been determined essentially in only two investigations (McKinney and Belcher, 1963; Deng and Knauss, 1997). An investigation by Lin and Nolle (1989) partially confirmed the findings of McKinney and Belcher using the same measurement method, but only as a function of temperature over a very limited frequency range. Other researchers

(Heydemann, 1959; Wada *et al.*, 1960; Kästner and Pohl, 1963) have attempted measurements of the bulk response of several polymer systems using wave propagation methods. However, these measurements did not provide accurate information because of insufficient precision in the measurement techniques.

McKinney and Belcher (1963) measured the viscoelastic bulk response of Poly (Vinyl Acetate) (PVAc) over a considerable range of temperatures, pressures and frequencies. However, one particular question surrounding their work was the unusually low glass temperature of 16.9 °C ascribed to their material (T_g for PVAc is usually measured as around 30 °C). Deng and Knauss (1997) re-examined this behavior at atmospheric pressure over a similar temperature and frequency range. While the two bulk measurements agreed in the bulk rubbery domain, they differed somewhat in magnitude across the transition range and in the glassy domain. Moreover, Deng and Knauss observed a wider transition range for the bulk response which was comparable to the transition extent exhibited by the shear response, contradicting the general notion of fewer relaxation times in bulk deformation vis-à-vis shear.

Our primary objective in this study is to explore the dynamic bulk behavior of Poly (Methyl Methacrylate) (PMMA). In Section 1.3, we discuss briefly the experimental method and the apparatus used, along with changes introduced subsequent to the investigation by Deng and Knauss (1997). Prior to considering measurement on PMMA we delineate the repeat measurements on PVAc in order to evaluate the precision of the measurement methods, as well as extending them to elevated pressures in Section 1.4. This is followed by the measurement results on PMMA over an extended range of temperatures and frequencies in Section 1.5 which is then compared to the transition

behavior of PMMA in shear along with the respective time-temperature shift factors in Section 1.6. We also present a comparison of these bulk compliance data with the other bulk data for PMMA available in the literature. We also summarize a comparison of the current experimental results with molecular dynamics simulations reported in detail elsewhere (Sane *et al.*, 2000). An overview in Section 1.7 concludes the presentation.

1.3 Experimental Preliminaries

Among the several means possibly useful for determining viscoelastic bulk response, including the recently developed method by Ma and Ravi-Chandar (2000), the Belcher/McKinney method (McKinney *et al.,* 1956) of measuring the dynamic compliance with the aid of piezoelectric volume sensitive drivers and sensors appeared at this time the most tractable for determining small deformation and time-dependent bulk response. The technique employs a small cavity in a (nearly) rigid solid containing the polymer specimen, a non-conductive fluid and two piezoelectric transducers, one serving as a volume expander and the other as a pressure sensor. A sinusoidal voltage applied to one transducer causes commensurate time-dependent pressure variations, which then interact with the second piezoelectric element (pressure sensor). The lengths of the stress waves associated with the applied frequencies are much larger than any of the cavity dimensions. Under these conditions, the (volumetric) deformation of the sample in the cavity occurs under essentially quasi-static hydrostatic pressure.

Based on the Belcher/McKinney method, an experimental apparatus along with updated electronic circuitry was developed in our laboratory (Deng and Knauss, 1997). Its central part is a thick-walled pressure chamber, shown in figure 1.1, forming a small

cylindrical cavity that contains the two piezoelectric transducers, an electrically non-conducting pressure-transmitting oil and a test sample as shown in figure 1.2.[2] The dynamic bulk compliance of the polymer sample is determined from equation 1.1 (see McKinney *et al.*, 1956, for more details).

$$\left(\frac{E_1}{E_2}\right)^* = A\left[C^* + \left(M_S^* - M_t\right)V_S\right] \qquad \text{(1.1)}$$

where E_1 and E_2 are, respectively, the complex voltages (including phase shifts) on the input (driver) and output (sensor) piezoelectric transducers, respectively; M_S^* and M_t are the complex bulk compliance of the specimen and of the pressure transmitting oil, and V_S is the volume of the specimen. A and C^* are constants that depend on the structure of the cavity, temperature, static pressure, frequency, and are determined through suitable calibration. In fact, the key to meaningful measurements is a careful calibration of the apparatus over the desired range of temperatures and frequencies, because the results of the method rely on small differences between large numbers. The calibration is accomplished with the aid of specimens possessing known properties. At a desired temperature, two runs cover the frequency range of interest. In the first, the cavity is filled with the pressure transmitting oil only ($V_S = 0$) and in the second run, an iron sample of known volume replaces the same volume of the pressure transmitting liquid. The bulk compliance of iron is 0.587×10^{-11} m^2/N and independent of temperature in the range of these studies. From the two runs, the constants A and C^* are determined.

[2] We are indebted to C. Schultheisz, formerly a post-doctoral fellow at Caltech and now at NIST, for the initial design of the pressure chamber.

The experimental set-up and the calibration procedure is described in detail by Deng and Knauss (1997); it served also as the basic equipment for the present measurements. However, the equipment was modified in several aspects to make it suitable for measurements at higher temperatures.

The earlier study on PVAc by Deng and Knauss as well as the measurements delineated here in Section 1.4 covered a temperature range of 25 – 65 °C. To perform experiments on PMMA, which possesses a glass transition temperature of T_g =105 °C, it was necessary to increase the temperature capability of the apparatus. As reported by Deng in his thesis (1997), the experimental set-up posed two challenges for high temperature measurements. First was the lack of experimental data on the bulk compressibility of the pressure transmitting oil (Di-2-ethylhexyl sebacate) beyond 75 °C. The second challenge derives from the fact that the voltage across the output transducer decreases significantly with increasing temperature. For example, the observed output voltage is approx. 4mV (RMS) at 25 °C for a 5V (RMS) input to the driver transducer, which decreases to less than 2mV (RMS) at 100 °C. The low output voltage of the transducer at higher temperatures is mainly attributed to the increase in the bulk compressibility of the pressure transmitting oil, which in turn decreases the hydrostatic pressures within the cavity. The transducer properties remain constant over the temperature range in this study. To obtain accurate bulk compliance measurements, it was thus essential to achieve a high signal-to-noise ratio. In the sequel we first describe the measurements for the adiabatic bulk compressibility of the pressure transmitting oil at temperatures beyond 75 °C. This is followed by the details of the modifications made to the experimental set-up.

1.3.1 Determination of the Adiabatic Bulk Compressibility of the Pressure Transmitting Oil

The non-conductive pressure transmitting oil used for the experiments was Di-2-ethylhexyl sebacate [Trademark: MONOPLEX® DOS] purchased from C.P. Hall Company.[3] It is the same oil employed by McKinney and Belcher (1963). The previous data on the bulk compressibility was available only to a temperature of 75 °C. To obtain the complement at higher temperatures, PVT and specific heat measurements were required over a suitable range of temperatures and pressures. To this end the oil was degassed under high vacuum prior to any measurements. Differential scanning calorimetry and high-pressure dilatometry techniques were used for specific heat and PVT measurements, respectively.[4] Figure 1.3 shows the temperature variation of the specific volume along an isobar. The values of specific volume and specific heat are listed in Tables A.1 and A.2 in Appendix A. The Tait equation (Brandrup and Immergut, 1989) equation (1.2), was used as the equation of state.

$$v(p, T) = (b_1 + b_2 T)\left[1 - 0.0894\ \ln\left(1 + \frac{p}{b_3\, e^{-b_4 T}}\right)\right] \qquad \text{(1.2)}$$

Here v is the specific volume, p the pressure and T the absolute temperature. [SI units]

The parameters b_i were determined with the aid of a least-square regression analysis as

$b_1 = 1.25 \times 10^{-3}\ m^3/kg$ $\qquad$ $b_2 = 8.67 \times 10^{-7}\ /K$

$b_3 = 6.27 \times 10^{7}\ Pa$ $\qquad$ $b_4 = 5.12 \times 10^{-3}\ /K$

---

[3] The C.P. Hall Company, 311 South Wacker Drive, Suite 4700, Chicago, Illinois 60606

[4] The PVT and specific heat measurements were carried out by C-Mold Inc. (Warren Road Business Park 31 Dutch Mill Road, Ithaca, NY 14850). Similar measurements were performed by Datapoint Testing Services using the same method, which yielded, however, very different results. Appendix A provides more details on this note.

The adiabatic bulk compressibility (M_t) was calculated using the thermodynamic relation (Thompson, 1972)

$$M_t = M_{iso} - \frac{T v \alpha^2}{C_P} \qquad \text{——————} \quad (1.3)$$

where M_t is the adiabatic bulk compressibility, C_P is the specific heat, M_{iso} is the isothermal bulk compressibility, and α the volumetric thermal expansion coefficient

$$M_{iso} = -\frac{1}{v}\frac{\partial v}{\partial p}\bigg|_T, \qquad \alpha = \frac{1}{v}\frac{\partial v}{\partial T}\bigg|_p$$

Figure 1.4 shows the adiabatic bulk compressibility of the Di-2-ethylhexyl sebacate at atmospheric pressure as a function of temperature; Table A.3 in appendix A provides the numerical values. This data is in good agreement with the previously available data.[5]

1.3.2 Modification of the Experimental Set-up

The experimental set-up developed by Deng and Knauss comprised a pressure chamber containing a small cylindrical cavity, the attendant electronic circuitry and the oil connections. The pressure chamber is housed in an environmental chamber for temperature control. The electronic circuitry includes a dual digital lock-in amplifier (Model DSP SR830, Stanford Research Systems) and a charge amplifier to measure the voltage across the sensor transducer. The lock-in amplifier measures the in-phase and out-of phase signal relative to the reference signal. A function generator built into the lock-in amplifier provides the input sinusoidal voltage to the driver transducer. It can supply a maximum voltage of 5 V (RMS) over a frequency range of 0.001 Hz to 100 kHz. The

[5] The previous data on adiabatic bulk compressibility of Di-2-ethylhexyl sebacate was obtained from Dr. McKinney via personal communication.

experimental set-up was modified to make it suitable and reliable for high temperature measurements as discussed in the sequel.

The electrical feed-through assembly plays a crucial role in achieving electrical communication between the transducers in the cavity and the measuring circuitry. It must also provide absolute pressure sealing against (any slow) air or oil leakage. The design of the feed-through was modified to achieve higher reliability in terms of both electrical connections and pressure sealing. The new design of the feed-through is shown in figure 1.5.[6] It consists of a stainless steel threaded rod with tightening nuts on both ends with thin Teflon washers to achieve pressure sealing and electrical insulation. The assemblies have to be tightened with sufficient torque to form the pressure seal, but not so tightly so as to obviate electrical insulation. Checks for oil leaks and electrical insulation are accomplished with the aid of helium gas leak and electrical impedance tests, respectively. Once proper sealing and insulation are achieved, the piezoelectric transducers are mounted on to the electrodes. The new feed-through assembly simplified the procedure for achieving a trouble free electrical communication from the cavity to the measuring circuit giving a higher reliability.[7]

The layout of the modified experimental set-up is shown in figure 1.6. To increase the output voltage of the sensor piezoelectric transducer, especially for "high temperature" operation, the signal from the function generator was doubled by using a Hewlett Packard model 6827A amplifier. Thus the driver transducer received an input

---

[6] Refer to Appendix B for details on the feed-through assembly used by Deng and Knauss.

[7] It also increased the stiffness of the cavity marginally by introducing more volume of steel and thus reducing the volume of the pressure transmitting oil in it. This resulted in a small sensitivity increase in the output voltage of the piezoelectric.

voltage of 10V (RMS) increasing the output voltage from the sensor transducer to about 6mV (RMS) on an average over the temperature range of interest.

1.3.3 Test Protocol

The pressure chamber was housed in a Grieve HT-800 industrial temperature-chamber[8] operating on a Honeywell (model UDC 3000) controller. The temperature of the pressure chamber was monitored via a platinum resistance thermometer (Model 5613, Hart Scientific).[9] A hole, drilled two inches deep into the bottom half of the pressure chamber, received the thermocouple and was filled with vacuum grease to optimize thermal contact. The thermocouple tip was located approximately half an inch from the cavity, and, because of the large thermal mass of the pressure vessel, it measured the temperature very steadily near the cavity by means of a Hewlett Packard multimeter (model 3457A) with an accuracy of 0.05 °C. The pressure chamber typically required five to six hours to achieve thermal equilibrium.

Gas bubbles were observed rising in the oil at temperatures above 80 °C, even after degassing the oil under vacuum for 12 hours at room temperature. Consequently, the oil was degassed at a temperature of 90 °C in a vacuum of approximately 30 microns (~ 0.03 mm Hg) until no further bubbling was detected. This degassing process requires about 12 to 15 hours per liter.

Data acquisition was computer controlled (IBM AMD-K6, 350MHz) through a serial communications with the SRS lock-in amplifier with communication achieved through a software program developed in Qbasic: The computer sends out a command to

[8] The Grieve Corporation, Round Lake, Illinois 60073-9989
[9] Hart Scientific, 799 E. Utah Valley Drive, American Fork, Utah 84003-9775

set the frequency of the function generator, then waits for 30 seconds before it starts recording the in-phase and out-of-phase voltages from the sensor transducer. The voltages are sampled 30 times for 30 seconds, then averaged to minimize random errors and stored on a hard disk. This procedure was repeated at each temperature for each frequency between 2 and 5000 Hz. However, due to poor responses at high (cavity incipient resonance) and low frequencies (unreliable response of the charge amplifier), only data between 10 and 1000 Hz were processed. The selection of the temperature range is based on the glass transition temperature. To reduce the effects of random experimental errors further, fourth-order polynomial segments were fitted to the data to smooth the connections between data points. As an illustration of the data quality, figure 1.7 shows the in-phase and out-of-phase voltages for the case of the oil-iron calibration over a temperature range of 27° to 123 °C.

1.4 Results on PVAc

In order to assess possible effects introduced into the apparatus by the modifications, the bulk response of PVAc was re-examined and the results were compared with those reported by Deng and Knauss (1997). In addition, measurements were made on PVAc under elevated static pressures to explore the effects of pressure on the bulk behavior.

1.4.1 Specimen

The PVAc specimen was purchased prior to this study from the Aldrich Chemical Company: It had a density of 1.191 g/cm^3, an average molecular weight of 167,000 and a glass transition temperature of 30 °C as quoted by the manufacturer which agrees closely with the value of 29.5 °C determined by Heymans (1983) on identical material. Deng and

Knauss used specimens from the same batch. They were irregularly shaped pellets ranging in weight from 0.1 to 0.3 gram. The specimen volume was determined from the specimen weight and the known specific volume as a function of temperature and pressure (Heymans, 1983; McKinney and Goldstein, 1974). The weight of the specimen was checked repeatedly before and after each experiment to detect any swelling or oil absorption with a digital balance (Mettler Ae240) using a precision of 1mg. The weight of the specimen remained constant within the resolution of the balance even after long exposure to the oil at all temperatures and pressures.

1.4.2 Measurements on PVAc at Atmospheric Pressure

Measurements at atmospheric pressure and over a temperature range of 20° to 50 °C yielded the storage and loss bulk compliances in the frequency range of 10-1000 Hz as shown in figure 1.8. At these frequencies a prominent change in the bulk compliance (storage part) was observed between temperatures 30-40 °C. Above and below this temperature range, the bulk compliance remained fairly constant, representing glassy behavior (lower temperatures) and rubbery behavior (higher temperatures).

The data in figure 1.8 was shifted according to the time-temperature superposition principle to produce a master curve; storage and loss parts were shifted by the same amounts. The reference temperature was chosen as 35 °C. Figures 1.9 and 1.10 show the master curves and the corresponding shift factors for the present data and their comparison with the data of Deng and Knauss.

While the overall nature of the bulk behavior of the present data is in agreement with the previous measurements, there is a distinct difference in the storage compliance. In addition to a probably minor difference in magnitude, the primary discrepancy appears

as a shift along the frequency axis. If one shifts the present data to the left by one and three-quarter decades, the two curves overlap to within the measurement resolution. The shift factors and the loss compliance on the other hand, are in fairly good agreement. In addition, the present data confirms the long transition zone (approximately eight decades) in bulk deformations reported by Deng and Knauss.

One probable explanation for the difference in the storage is a difference in the moisture content of the specimens inasmuch as the specimens had been stored at approximately 5 °C in a Polyethylene container since the previous study (three to four years). Knauss and Kenner (1980) demonstrated that realizable though small changes in the moisture content of a specimen effect the thermo-mechanical properties in a similar manner as those caused by changes in the temperature. Based on the data of Knauss and Kenner (1980), one infers that an increase of 0.5% in the absorbed moisture levels of the specimen is sufficient to account for this time shift. Because it is reasonable that the PVAc specimens gained 0.5% moisture over a period of four years when stored in a refrigerator, the relative shifts of the two sets of data are consistent.[10]

1.4.3 Bulk Response at Elevated Pressure

To assess the effect of pressure on the bulk behavior, measurements were carried out on PVAc over a temperature range of 30° to 50 °C under superposed pressures of 500psi (~ 34 atm), 1000psi (~ 68 atm) and 1500psi (~ 102 atm). The pressure chamber was allowed

[10] The experience with moisture content and personal discussion with Prof. D. Plazek indicated that PVAc is extremely difficult to "dry out" after moisturization. The only means of obtaining dry PVAc appears to be appropriately tailored synthesis.

to attain thermal equilibrium at each temperature, keeping both the inlet and outlet ports of the cavity open. Then the outlet valve (located physically at the top of the chamber) was closed first and the chamber was charged to the desired static pressure, after which the inlet valve (located at the bottom) was closed to isolate the chamber from the pressure supply and the environment. The pressure was monitored near the inlet port. The apparatus was calibrated over the desired pressure and temperature range using the procedure outlined in Section 1.3.

Master curves at different pressures were obtained again as displayed in figure 1.11, by shifting the storage and the loss parts by equal amounts. The shift factors did not change over this pressure range, their spread falling within the uncertainty limits of the shift factors reported in figure 1.10. One observes that the storage compliance decreases systematically with an increase in static pressure. No significant effect of pressure was observed on the loss compliance, although a proportionally small fractional change would hardly be measurable with the current apparatus. McKinney and Belcher (1963) have reported similar measurements over a much wider pressure range (0-980 atm). In the present data the storage compliance decreased on average by 8% in the transition range for an increase in pressure of 102 atm. McKinney and Belcher observed a change of about 10% in transition over a pressure increment of 98 atm signifying fair agreement of the two data sets to the extent they overlap.

1.5 Results on PMMA

A successful repetition of measurements on PVAc implied that the modified experimental set-up was functioning properly. Measurements on PMMA were carried out only at

atmospheric pressure. Attempts were also made to study the bulk behavior of Polystyrene (PS) with a glass transition temperature of 100 °C. But Polystyrene dissolved in Di-2-ethylhexyl sebacate at elevated temperatures. Here we report the measurements on PMMA.

1.5.1 Specimen

The PMMA, used also in a previous study (Lu *et al.*, 1997), was purchased from ACE Company (ACE, now a part of Ono). The glass transition temperature was quoted as 105 °C by the manufacturer. Like the PVAc material the PMMA specimens were also irregularly shaped pellets ranging in weight from 0.1 to 0.3 gram. The specimen volume was again determined from the weight of the specimen and the known specific volume as a function of temperature (Brandrup and Immergut, 1989). The weight of the specimen was monitored using again the digital balance (Mettler Ae240); and was also found to remain constant within the resolution capability of the balance even after long exposure to the oil at different temperatures.

1.5.2 Measurements

The overall motivation for performing bulk modulus determinations is driven by a desire for better understanding the mechanical properties characterization of polymers. A part of that endeavor is the examination of thermo-mechanical response, including the phenomenon of physical aging. We allude to this effect here because we could observe in these studies the importance of including or being aware of the effects of physical aging on the volumetric response of polymers in general and of PMMA in particular.

1.5.2.1 Inconsistent Data and Physical Aging

Initial measurements on PMMA produced seemingly inconsistent results. These preliminary data for the temperature range from 65° to 105 °C and frequencies of 10 to 1000 Hz are shown in figure 1.12: The storage compliance did not increase in a consistent manner with an increase in the temperature, as one would expect. This inconsistency was traced to the thermal history of the samples.

During these measurements the pressure chamber was thermally equilibrated at a desired temperature and the calibration runs were made using oil and the iron samples as before, followed by the measurements on the polymer sample. However, to repeat the process at a new temperature the polymer sample was removed from the cavity and air-cooled to room temperature, i.e., quenched, because of its small thermal mass. The next desired temperature was set and the procedure was repeated. This procedure subjected the PMMA sample to multiple cycles of relatively rapid heating and cooling which had a notable effect on volumetric response; this thermal history left its indelible impression, as is evident from a comparison with data deduced from a more controlled thermal history.

1.5.2.2 Annealed PMMA

The above finding establishes clearly that physical aging can significantly affect volumetric measurements, thus calling for a carefully controlled thermal history. Therefore, a sample was typically annealed prior to the measurements by holding it at 115 °C (10 °C above T_g) for nearly four hours in an oil bath (the same oil as the pressure transmitting oil) after which it was allowed to cool to room temperature at a rate of approximately 5 °C/hour. In addition, the experimental procedure was modified. The calibration runs were first completed over the whole range of temperatures and

frequencies. The measurements on PMMA samples were then carried out starting with the highest temperature and progressing to lower test temperatures without removing the sample from the cavity. To examine any possibly remaining effects of physical aging, data was collected at regular intervals and at each temperature over a span of 30 hours. No systematic shift in the data was observed with time, indicating that physical aging was not prevalent if this conditioning procedure was followed.

Measurements were made over the temperature range from 123° to 27 °C. The storage and loss compliance over the frequency range of 10-1000 Hz is shown in figure 1.13. The numerical values of the storage and loss compliance data are listed in Tables C.1 and C.2 in Appendix C. Measurements were carried out on multiple samples and were repeated again thirty times to reduce random errors. These averaged values of bulk compliance were quite repeatable for temperatures below 71 °C. However, uncertainties increased up to ± 5 or 6% as temperatures approached the glass transition temperature. The maximum values of uncertainties were observed at high temperatures and low frequencies.

The major transition of the storage compliance occurs at temperatures between 81° and 123 °C. Beyond 123 °C, PMMA is expected to approach the bulk rubbery domain.[11] At temperatures below 40 °C the bulk compliance changes slowly with frequency, and the loss compliance remains virtually constant; this represents the glassy domain. Because the loss compliance was very small its accuracy at temperatures above 81 °C and at the lower frequencies is low. At high temperatures, negative values for the loss compliance were sometimes obtained.

Although the individual temperature segments did not exhibit monotonic changes in slope, an attempt was, nevertheless, made to shift the experimental data using the time-temperature superposition principle to obtain "most reasonable" master curves. Figure 1.14 shows the resulting curves relative to 105 °C. Both storage and loss compliance data were shifted by identical amounts. The corresponding shift factors are shown in figure 1.15. It was observed that the bulk compliance data shifts well for temperatures below 92 °C. However, beyond this temperature the curvatures of both the storage and loss compliance data did not match very well and it was therefore not reasonable to assign a degree of reliability to the shifted data in the high temperature range.

1.6 Comparison With Other PMMA data

We next report an evaluation of the current measurements relative to bulk and shear responses measured by other investigators. In addition we present a comparison between our experimental results and the results obtained from our parallel efforts to compute bulk compliance of PMMA by molecular dynamics simulations.

1.6.1 Comparison with Other Bulk Data

The shear and uniaxial responses of PMMA have been extensively studied in the past and attempts to compute the bulk response from the shear and uniaxial responses were generally not very successful (Lu *et al.*, 1997). There have been only few direct measurements of bulk response of PMMA though they did not reveal much information on the rate-dependent bulk behavior because the measurements were carried out under

[11] The current experimental set-up does not allow us to carry out reliable measurements beyond 123 °C due to beginning of thermal degradation of the pressure transmitting oil.

limited conditions, with either frequency or temperature as the only variable. Heydemann (1959) reported measurements over six decades of frequencies (0.1 to 60kHz) at room temperature, while Kono (1959) measured the bulk modulus of PMMA over a temperature range of 20 to 190 °C in the MHz frequency range. Lin and Nolle (1989) reported the dynamic bulk compliance of PMMA at 1000Hz and 12 atm. pressure over a temperature range from 0° to 58 °C. To visually compare these collective results, they are summarized in figure 1.16 together with an excerpt from the present data as a function of temperature and at the single frequency of one kHz.[12]

For reference purposes we also show in figure 1.16 a comparison of our molecular dynamics computations of the bulk compliance of PMMA[13] with the current experimental data. For the computations, models of amorphous PMMA were built using Cerius, a molecular modeling software program, and NPT dynamics were imposed on the model to compute the bulk compliance as a function of temperature. Fairly good agreement is observed between the present data, the data from the computations and Kono's data in the glassy domain (low temperatures). One can also appreciate the effect of time-temperature shift by comparing the data of Kono (one MHz) and those of Lin and Nolle (one kHz). Also, in the present data the transition is observed around 80 °C for an experimental frequency of 1 kHz, while in Kono's data (measurements made at 1 MHz), the transition shifts to a higher temperature. In contrast to most of the data, the computations predict a constant bulk compliance over the temperature range in figure 1.16. It must be remembered, however, that the computations provide information at very high

[12] For comparison purposes, the bulk compliances gleaned from the literature were determined by inverting the corresponding bulk modulus data.
[13] This is the subject of a separate publication; see Sane *et al.*, 2000.

frequencies, namely on the order of giga hertz (or very small time scales, on the order of nano-seconds) and at such high frequencies, the material may well respond in a purely glassy manner over the current temperature range.

1.6.2 Comparison with Shear Response

The relaxation mechanisms and molecular rearrangements accompanying bulk or shear deformations have always been of general interest to researchers. It is often believed that the relaxation mechanisms controlling bulk deformations depend only on very local motions of the polymer molecules and that long range entanglements and cross-links play no or a subsidiary role. In contrast, the shear behavior is supposed to be governed by local as well as long range molecular interactions and rearrangements. Thus it has been argued that the bulk response should exhibit a narrower transition zone compared with the shear response. With this perception in mind, we present in figure 1.17 the real part of dynamic shear compliance and the real part of the dynamic bulk compliance at 105 °C. The dynamic shear compliance was computed from the shear relaxation data reported by Lu *et al.* (1997) for the same ACE PMMA. One observes that the bulk response exhibits a transition over (at least) eight decades, which is comparable to the transition range shown by the shear response. In view of the fact that -because of experimental limitations- there is no clear indication of the glassy or rubbery response domain, this range must be considered to be a lower bound.

Deng and Knauss (1997) have made the point that the transition for the bulk compliance does not fall into the range of the transition of the shear behavior, but occurs essentially in the domain of the glassy shear response; in addition, they note that the time

scales of the two transitions are on the same order. Certainly, the transition length of the bulk response was not significantly or not at all shorter than that of the shear behavior.

The similar comparison for the PMMA data suggests a more descriptive connection that hinges on the concept of short and long-range molecular motion in any time dependent behavior. We first note from figure 1.17 that, like for the PVAc data, the range of the bulk transition is as extended as the transition of the shear response; both range over about eight decades. On the other hand, because of instrumentation limitations the "rubbery" and "glassy" domains of the bulk response are not clearly identified. However, in contrast to the PVAc data, the bulk and shear responses for PMMA exhibit closely the same slope on comparable log-scales in what one normally considers to be the glassy domain.

For further discussion we define short-range interactions between units in a chain and its surroundings as those that involve only a short segment in a molecule chain and which occur uncoordinated with segments that are many units removed form the point of activity. While the precise number of "small" is debatable, the distinction of "long-range interaction" clearly is the counterpart and requires coordinated interaction or sequenced activity involving many units along the chain backbone. Thus, long-range interactions typically require longer time scales than short range interactions and one may identify short-range interactions with a short time scale, and long term interactions with the longer times in a spectral distribution.

On physical grounds one expects that bulk response involve primarily short-range interactions. Similarly, the glassy domain of the shear behavior is also readily identified with short-range mobility, while motions in the shear transition region involve

increasingly longer interaction distances along the molecule chain and thus longer relaxation or retardation times. These observations are consistent with both the PVAc and the PMMA data available to date.

We have already referred to the fact that the glassy domain in the PMMA shear data is influenced by the β-mechanism. We note from figure 1.17 that the bulk data in that domain are roughly proportional to the shear response, so that the suggestion is close at hand that the same molecular mechanisms or molecular building blocks are at play. In other materials, as, *e.g.*, PVAc, this proportionality is not equally clear and may, realistically, not be measurable. Recall that determining the bulk behavior requires measurement techniques that offer a very high precision relative to those normally employed for measuring shear or uniaxial behavior. Variations in the glassy domain, which are less than one percent of the whole transition amplitude, can hardly be expected to be recorded: The short range behavior governing the bulk response experiences a transition amplitude of only a factor of three to four, which is very small compared to the shear transition difference which spans two to three orders of magnitude. Thus the bulk variation is only a very small fraction of what is characteristic for the shear behavior. Accordingly, one might expect that for most materials possessing a distinct "glassy domain" [constant shear or uniaxial modulus/compliance as a function of time or frequency], the true variation is difficult to assess by standard experimental means, but becomes apparent, at least qualitatively, only by way of the bulk behavior. This observation leaves open the question as to whether the same chain segments or side groups on the chain are responsible for the glassy shear and for the bulk response.

The idea that different molecular, configurational deformations control bulk and shear response in PMMA is supported by the comparison of the shift factors for the bulk and shear behaviors in figure 1.15. The solid data points represent the shift factors derived from forming the bulk compliance master curve in figure 1.14, while the open symbols represent the shift data derived in producing the shear modulus data in figure 17 (Lu *et al.*, 1997). Note that the bulk shift factor varies approximately linearly with temperature, a characteristic for Arrhenius behavior, although the bulk shift factors appear to begin deviating (slightly) from the linear behavior beyond T_g, while the shift factors for shear exhibit a more distinctly nonlinear variation. Similar differences in the behavior of the bulk and shear factors were observed by Deng and Knauss during their investigation of PVAc.

In this context a concern regarding the time-temperature superposition principle arises. As mentioned earlier, the storage component of the bulk compliance shifts relatively well for temperatures below 92 °C, however beyond this temperature the rationale for shifting is less clear. This could have two possible explanations: one derives from the uncertainties in the measurements at high temperatures, which cannot unequivocally resolve the curvatures of the data segments at these temperatures. The other arises from the question of the validity of the time-temperature superposition principle, when applied to the bulk behavior of PMMA. Anomalies in the application of reduced variable methods have been reported by Ferry *et al.* (1957) during investigations of the dynamic shear properties of several methacrylates. The failure of the method of reduced variables was attributed to the presence of a secondary relaxation mechanism (or β relaxation involving side chain motions). The temperature dependence of the relaxation

times associated with this secondary mechanism is different from that for the primary mechanism (the α relaxation, involving mostly chain backbone motions). The reduced variable method can be applied only in the ranges of temperature and frequency where the compliance contributions of the secondary mechanisms are comparatively negligible. This secondary relaxation mechanism has been observed in PMMA by several investigators, namely by Iwayanagi and Hideshimna (1953), Deutsch *et al.* (1954), and by McCrum (1967). The β relaxation region in PMMA is observed at temperatures below its glass transition temperature and the β transition temperature varies from 20 °C at 1 Hz to 90 °C at 1 kHz.

In our PMMA measurements the temperature and frequency range covered overlaps with the β transition range. The molecular formula of PMMA, illustrated in figure 1.18, indicates the presence of an ester side group, which is relatively massive. The molecular contributions to the bulk deformations in PMMA in these measurements could be derived primarily from the motion of the ester side groups coupled with the motion of the chain backbone, with, however, the rotations and oscillations of the side groups playing a dominant role. With the present apparatus, measurements at higher frequencies (incipient cavity resonance) and temperatures (thermal degradation of the pressure transmitting oil) were inaccessible and it was therefore not possible to make a clear distinction between the contributions from the primary and secondary relaxation mechanisms to bulk deformations.

1.7 Concluding Remarks

We have re-examined the bulk response of Poly (Vinyl Acetate) and studied that of Poly (Methyl Methacrylate) over a range of temperatures and frequencies. The results on PVAc are in agreement with similar results reported by Deng and Knauss (1997) if one allows for differences in moisture content of the specimens. The bulk response of PMMA exhibits a transition domain over at least eight decades, which is on the same order as the transition domain observed in its shear response. This observation agrees with the same finding for PVAc and contradicts thus the general notion that bulk deformation involves fewer relaxation times than shear deformations. Moreover, even though the data does not necessarily represent the complete transition range for the bulk response of PMMA, the centers of the transitions for shear and bulk responses occur at different frequencies, as was found to be true for PVAc. This as well as differences in the behavior of the shift factors for bulk and shear responses supports the idea that different molecular mechanisms control these two types of deformations.

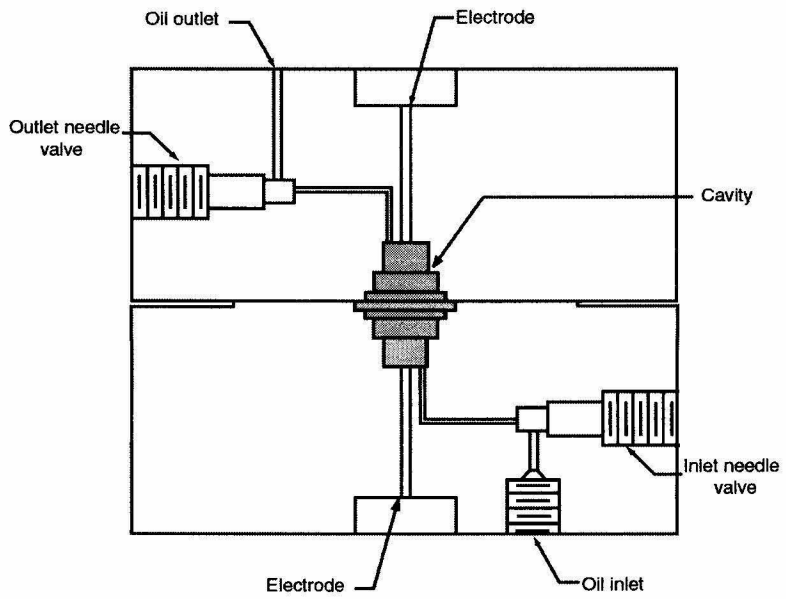

Figure 1.1: Schematic of the pressure chamber.

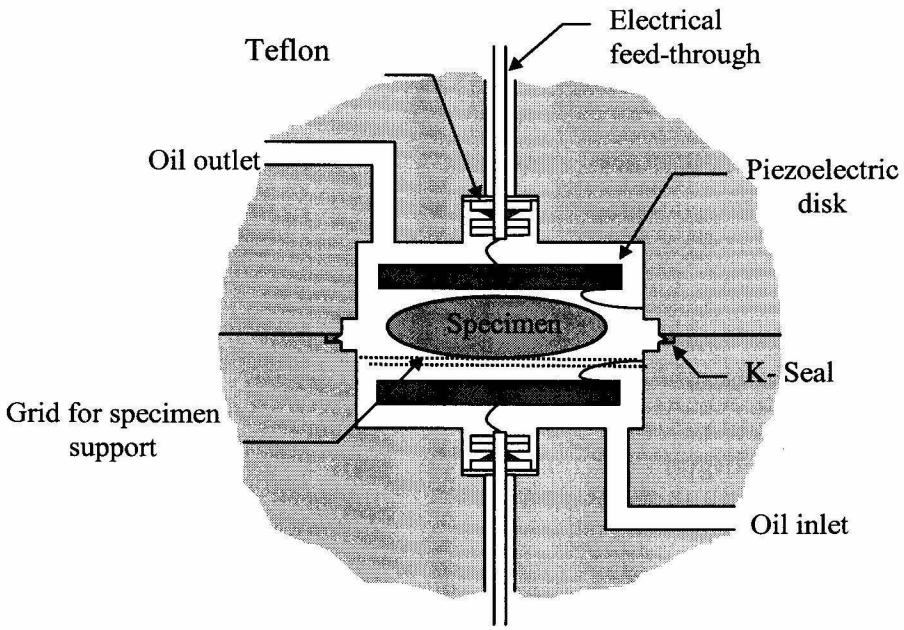

Figure 1.2: Cavity and piezoelectric transducers.

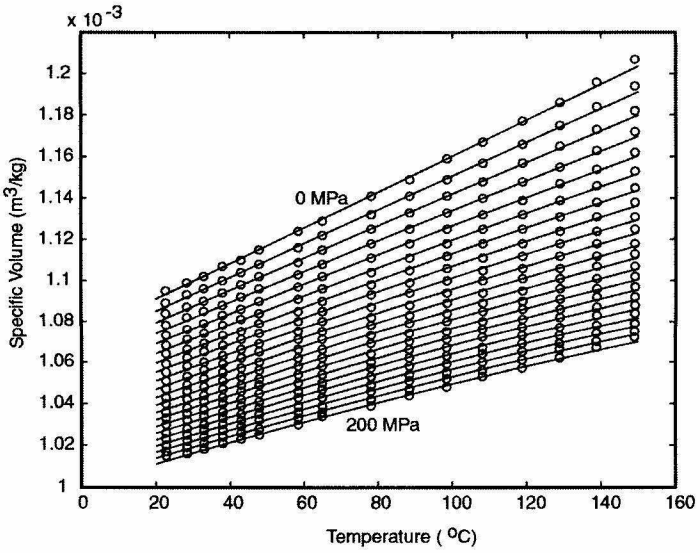

Figure 1.3: PVT data of the pressure transmitting oil (Di-2-ethyl-hexyl sebacate) in 10 MPa increments.

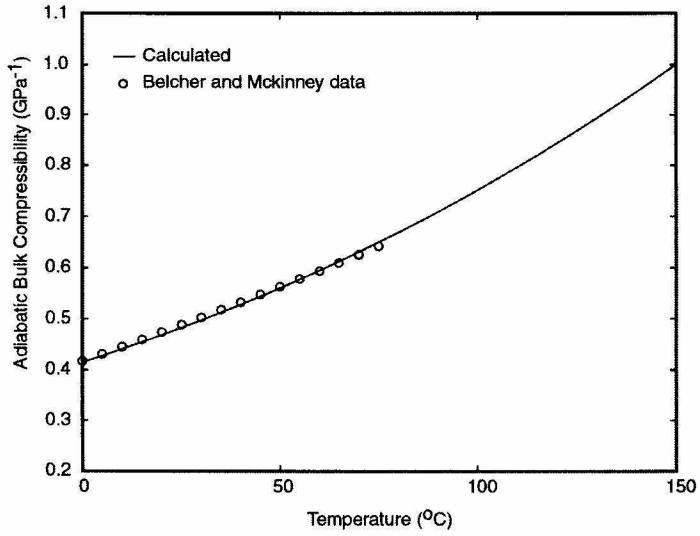

Figure 1.4: Comparison of the adiabatic bulk compressibility of the pressure transmitting oil as calculated from PVT data (figure 1.3) with Belcher and McKinney data (obtained from J.E. McKinney via personal communication).

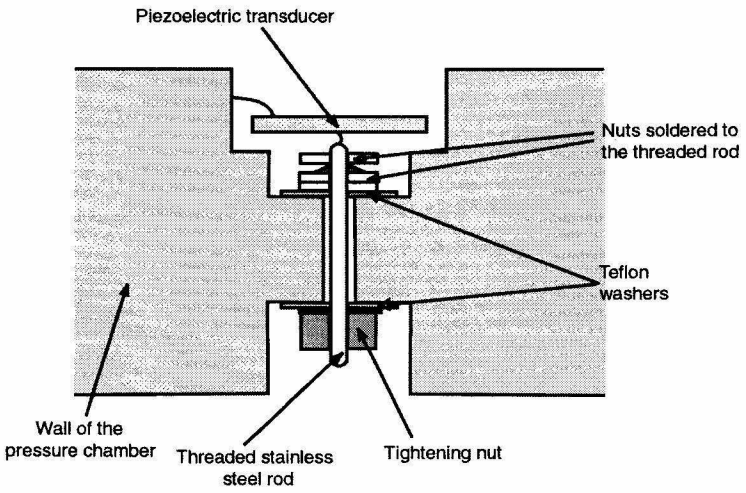

Figure 1.5: Electrical feed-through.

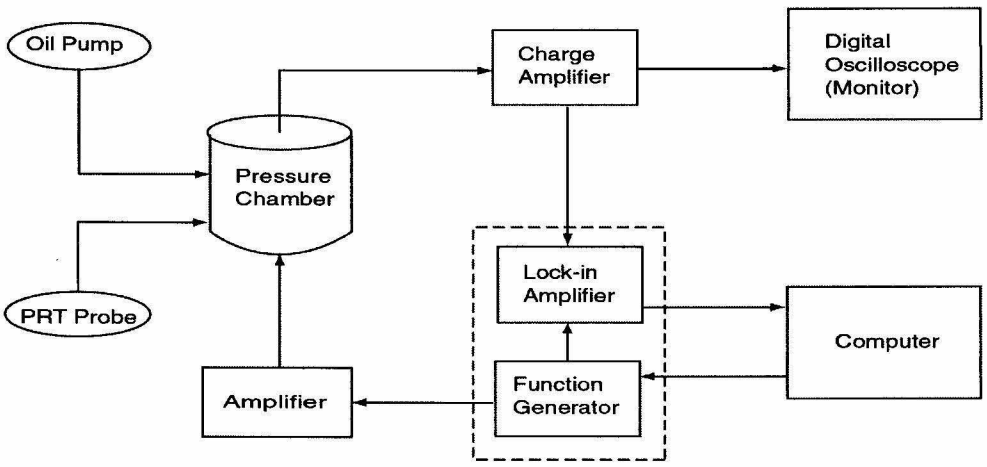

Figure 1.6: Experimental set up.

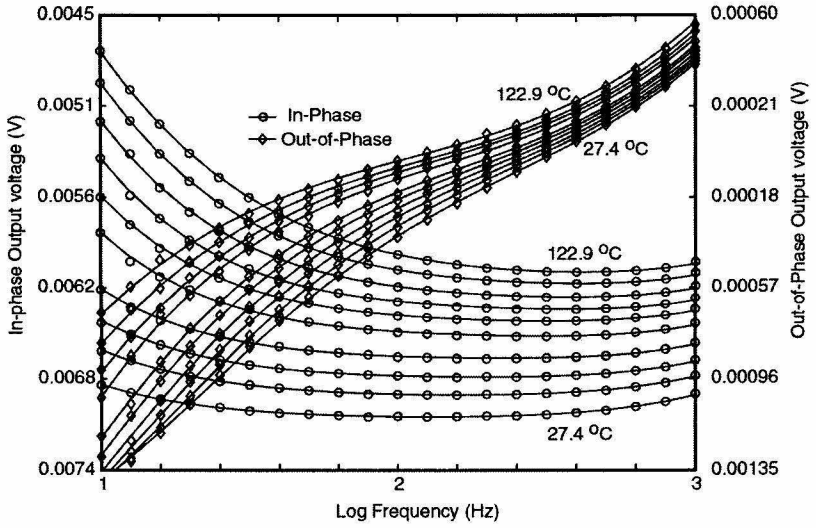

Figure 1.7: Example of in-phase (left ordinate) and out-of-phase (right ordinate) output voltages for oil plus iron sample in the cavity at the temperatures 27.4, 38.6, 49.3, 60.2, 71.0, 81.7, 92.1, 102.4, 112.8 and 122.9 ^{0}C.

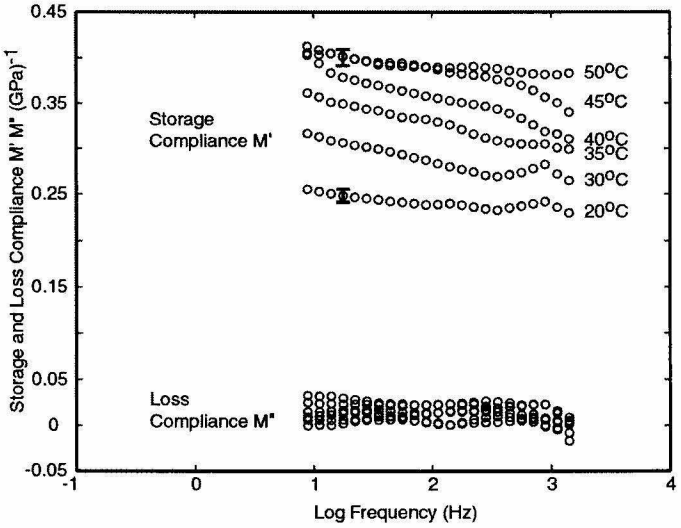

Figure 1.8: Storage M′ and loss compliance M″ of PVAc at indicated temperatures as a function of frequency. Note error bars indicating extent of typical data variation.

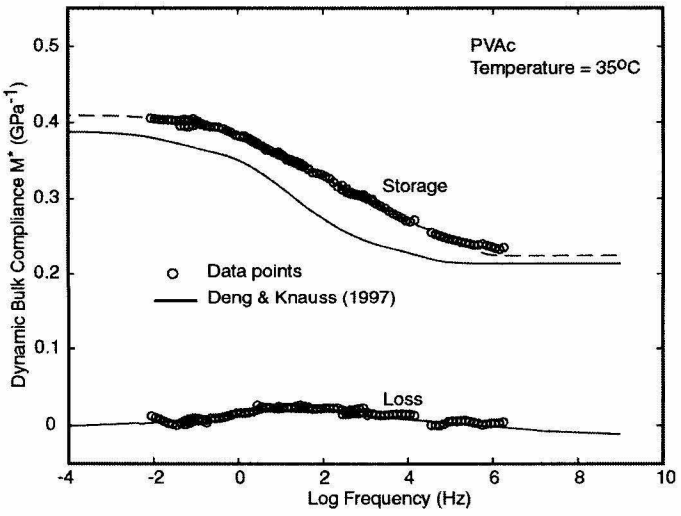

Figure 1.9: Bulk compliance of PVAc; comparison with data of Deng and Knauss (1997).

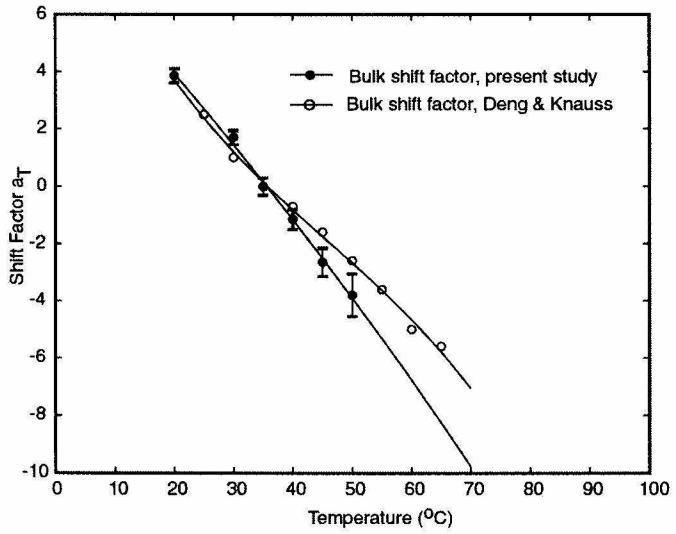

Figure 1.10: Shift factors for the bulk comliance; comparison with data of Deng and Knauss (1997).

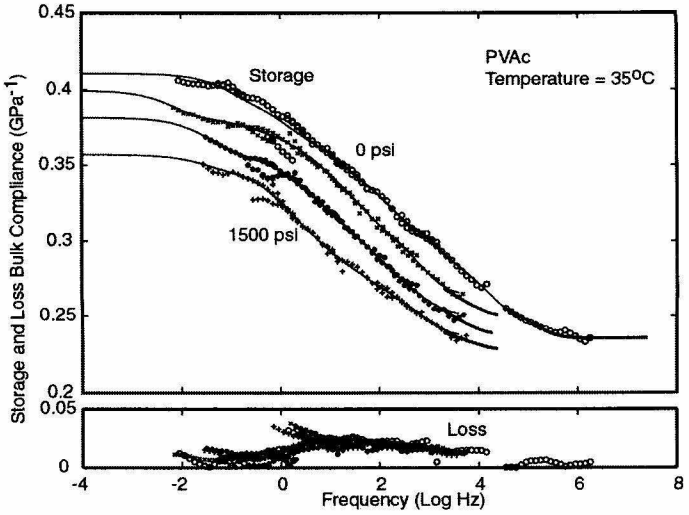

Figure 1.11: Variation of the bulk compliance of PVAc with superposed pressure. The storage compliance data at higher pressures is shown by shifting the data vertically with respect to 0 psi data for clarity. The shift is made by adding –0.01 to 500 psi data, -0.025 to 1000 psi data, and –0.035 to 1500 psi data.

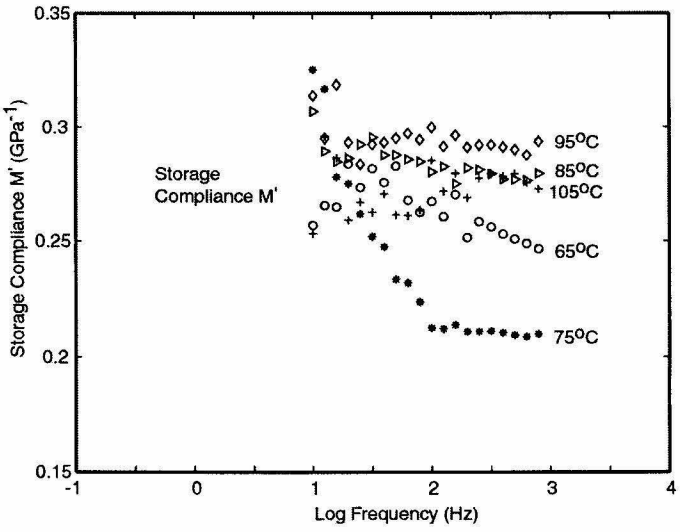

Figure 1.12: PMMA bulk compliance; inconsistent results when physical aging is neglected.

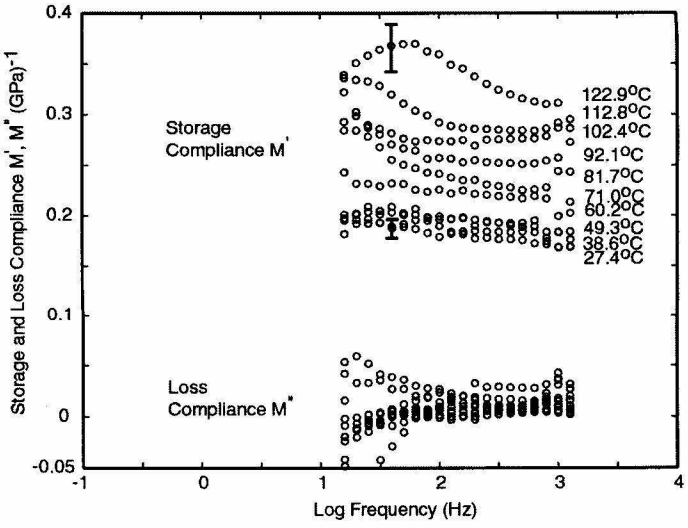

Figure 1.13: Storage M′ and loss compliance M″ of PMMA at indicated temperatures over two decades of frequency. Note error bar estimates at extreme temperatures.

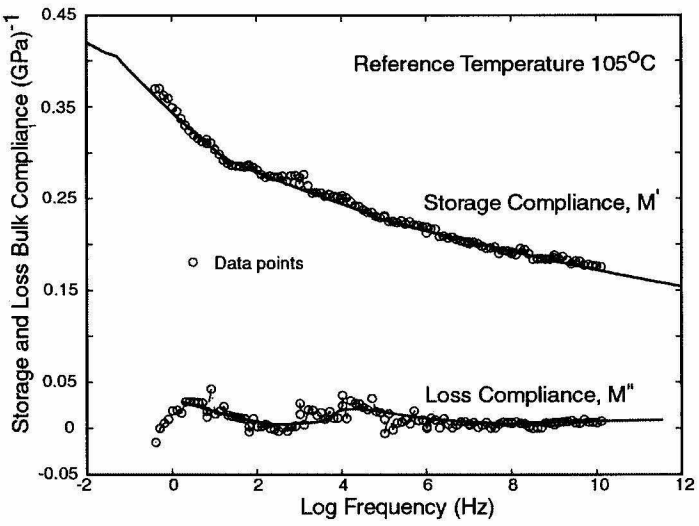

Figure 1.14: Master curves of storage and loss bulk compliances for PMMA at a reference temperature of 105 ^{0}C.

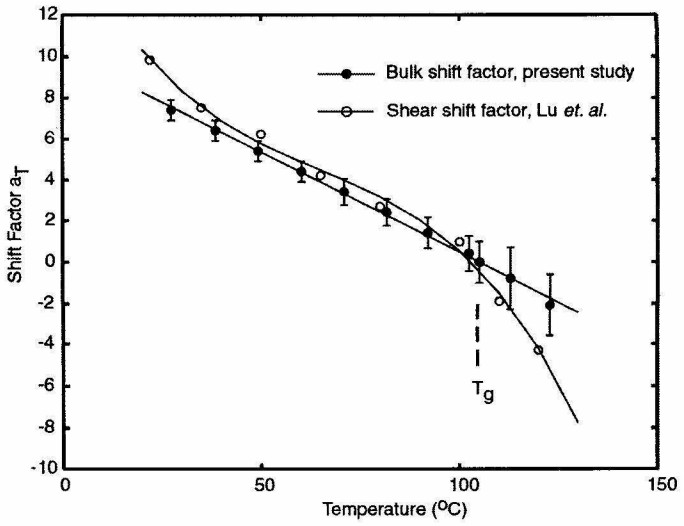

Figure 1.15: Comparison of the shift factors for the bulk compliance of PMMA with that for the shear compliance (Lu *et al.*, 1997).

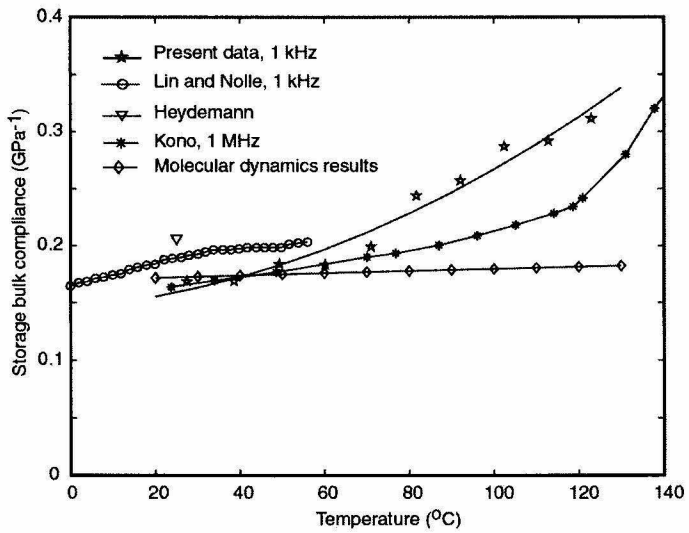

Figure 1.16: Comparison of bulk compliance of PMMA with data from the literature; a) present data at 1 kHz as a function of temperature with b) Lin and Nolle at 1 kHz, 12 atm pressure, c) Heydemann reported constant bulk compliance at room temperature and over a frequency range of 0.1 to 60 kHz, d) Kono at 1 MHz, e) Computational results using molecular dynamics simulations.

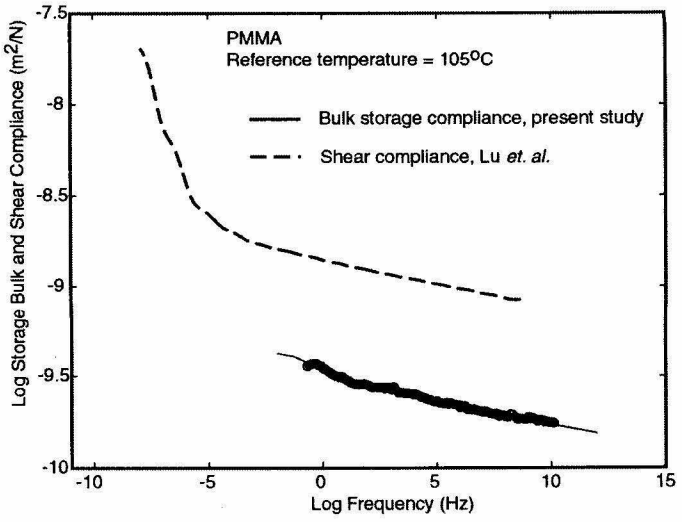

Figure 1.17: Comparison of shear and bulk compliances for PMMA. Lu *et al.* (1997) used the identical PMMA material as in the present study.

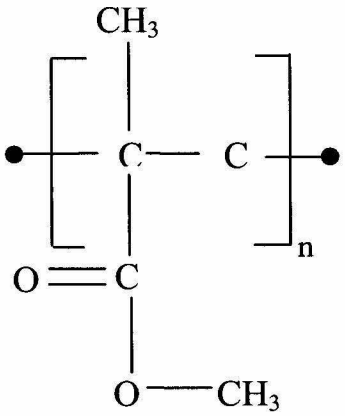

Figure 1.18: The molecular formula of PMMA.

Chapter 2

Molecular Dynamics Simulations to Compute the Bulk Response of Amorphous PMMA

2.1 Abstract

The results of molecular dynamics computations and corresponding values of laboratory measurements are compared to assess the efficacy of the numerical method. Details are presented on the modeling process, including the selection of an appropriate force field derived from separate computations on isotactic (crystalline) PMMA together with commensurate experimental data. It is found that in addition to typical energy minimization and temperature annealing cycles to establish equilibrium models, it is advantageous to also subject the model samples to a cycle of a relatively large pressure excursion (GPa's), to further improve the equilibrium state. Although the computations are limited to small samples in a physical sense (three polymer chains with fifty monomer units per chain per unit cell containing 2256 atoms), it appears that the primary limitation of the comparison with experimental data rests in the very short times (picoseconds). Estimates based on the time-temperature superposition principle do not overcome this difficulty, but may, on the other hand, signify limitations of the time-temperature trade-off as normally practiced.

2.2 Introduction

The increasing power of digital computational methods has offered the potential for "molecular dynamics" simulations to predict the mechanical properties of amorphous polymers. Molecular dynamics provides the possibility of determining basic physical properties that are difficult or laborious to access in the laboratory. However, this approach can become established as a laboratory substitute only after a large number of situations are studied both numerically and experimentally in comparisons. At present the prediction of macroscopic properties using molecular models[14] is, at best, challenging and the question of the size of a numerical model for adequate property representation is of paramount concern. A number of studies have demonstrated the application of molecular simulation methods to compute (limited) mechanical properties of polymers (Fan and Hsu, 1992; Fan *et al.*, 1994; Karasawa and Goddard, 1995), and results obtained from these simulations have been encouraging since they agree rather well with the laboratory measurements. However, in most of these cases the comparison between the experiments and the simulations were made at only one temperature, usually at room temperature. It is well known that in polymers the physical properties change substantially with time and temperature. Surprisingly little attention has being given to study the mechanical properties as a function of temperature using molecular dynamics simulation techniques.

There have been a few efforts to study the relaxation behavior in polymers using molecular dynamics techniques (Fan *et al.*, 1997). However, these investigations were concerned with mostly local and short time relaxation phenomenon through equilibrium

[14] Simulated structures are composed of limited number of atoms.

MD. Long time chain relaxation processes are certainly beyond the scope of the conventional MD. Therefore, to explore complex properties such as uniaxial and shear response of the amorphous polymers requires treatment of these systems using non-equilibrium molecular dynamics techniques (Evans and Morriss, 1990; Gao and Weiner, 1996; Sarman *et al.*, 1998). To data, most of the studies involving NEMD is on the short oligomers of Polyethylene (10-20 carbon atoms per chain) and focussed on obtaining shear viscosity as a function of strain rates (Khare *et al.*, 1996; Lee and Cummings, 1998). Furthermore, the strain rates used in these studies were extremely high due to the time scales involved in the simulations. As a result of which the outcome from the simulations did not agree with the experiments.

It would seem that determining bulk response (pressure-volume) should be one of the more readily successful computations for physical property determinations using equilibrium MD, because it deals typically with small macroscopic deformations and possesses a (mathematically) one-dimensional deformation character, unlike the case in shear or uniaxial deformations. Thus, the object of the present study is occasioned by non-trivial bulk compliance measurements that have become available on a real amorphous polymer system, Poly (Methyl-Methacrylate) (PMMA), which is also widely used in engineering and for utility items. Because such measurements are extremely difficult and time consuming, the computation alternative appears attractive. However, acceptance of molecular dynamics as a laboratory substitute hinges on the successful demonstration of complete equivalence in results derived from numerical methods, one must demonstrate that both the temperature and time controlled features of polymer behavior are correctly rendered. As a start one may deal with the time-independent range;

however, that limitation needs to be narrowed in the future. The present computations are thus a valuable, initial model example for comparing molecular dynamics computations with experimental data. Consequently, we present here a comparison of such computations on bulk compliance as a function of temperature with laboratory measurements made on PMMA specimens, discussing, at the same time, the relation of these computations valid for only very short-times with the corresponding measurements acquired at much longer time scales.

The paper is organized by first giving the details of the simulation techniques and sample preparation procedure in Section 2.3. This is followed by a presentation of the experimental results on an amorphous PMMA system (Sane and Knauss, 2000) and those of the simulations in Section 2.4. We then present a comparison between the molecular dynamics simulation results and the experimental results. A summary in Section 2.5 concludes the paper.

2.3 Simulation Details and Sample Preparation

In this section we outline the simulation methodology. It includes first a selection of a proper force field to accurately describe various interactions of amorphous PMMA, following which the method of the model sample construction is delineated. Finally, details of the simulations are presented.

2.3.1 Selection of Proper Force Field

A main ingredient in MD calculations is the description of forces between atoms (neighbors/molecules) as their centers move relative to each other. This description is characterized by a force field, which can be considered for analytical purposes, to be a

collection of energy terms characterizing interactions between atoms of a system. The potential energy, E, of a generic force field for an arbitrary geometry of molecules is typically characterized by the following terms:

$$E = E_B + E_A + E_T + E_I + E_{vdw} + E_Q$$

The first four terms represents bond interactions, namely, bond stretching (E_B), bending (E_A), torsion (E_T), and inversion (E_I). The last two terms represents non-bond interactions, possessing van der Waals (E_{VdW}) and electrostatic (E_Q) character. Different functional forms may be used for these energy terms.

The realism of the computation results hinges on the commensurate choice of the force field, i.e., on the proper expressions for the energy terms. A large number of force fields are available in the literature, optimized to represent different types of physical systems. To represent amorphous PMMA, the three most commonly used force fields were examined, namely, Universal Force Field (Rappé *et al.*, 1992), Dreiding Force Field (Mayo *et al.*, 1990) and COMPASS (Sun, 1998).

In order to select the "best" force field from the three listed above, isotactic PMMA (iPMMA) was modeled. Isotactic PMMA is crystalline, yet a good structural analogue to amorphous PMMA, served, therefore, as an ideal structure for a force field evaluation because suitable properties obtained from X-ray structural analysis are available in the literature. The iPMMA crystals are orthorhombic with cell dimensions, a = 41.96 Å, b = 24.34 Å, and c (fiber axis) = 10.50 Å. Its molecular arrangement is represented by a double-stranded (10/1) helix (Kusanagi, *et al.*, 1994). The model structure was assembled using the atomic coordinates illustrated in figure 2.1. The response of the iPMMA crystal structure was evaluated for different force fields by carrying out a full optimization of the

atomic coordinates and cell parameters in comparison with the experimental data. To account for electrostatic interactions, the charges were derived from the QEq method (Rappé and Goddard, 1991). The PMMA monomer is shown in figure 2.2 along with the nomenclature used for the different atoms. The corresponding charges obtained from the QEq method are shown in Table 2.1. Ewald summation was used for computing the non-bonded interactions.[15]

Table 2.1: Charges (Coulomb) of different atoms in PMMA monomer unit.

C_1	-0.2411	C_3	0.6862	H_{1C5}	0.1888	H_{1C4}	0.1321
C_2	0.0213	O_2	-0.5136	H_{2C5}	0.0718	H_{2C4}	0.1751
H_{1C1}	0.1512	O_1	-0.5877	H_{3C5}	0.1677	H_{3C4}	0.1197
H_{2C1}	0.1087	C_5	-0.0930	C_4	-0.3872		

The crystal structure was first subjected to multiple cycles of energy minimization, followed by a comparison between the experimental and the simulated crystal data under the three different force fields, as illustrated in Table 2.2. From that table one observes considerable disagreement between experiment and simulation for the universal force field and hence it was discarded from further consideration. The crystal structure was then subjected to NPT dynamics[16] at 300 K and at atmospheric pressure using the Dreiding

[15] Ewald summation is a technique used for the calculation of non-bond interactions in periodic systems (Karawasa and Goddard, 1989).

[16] NPT dynamics implies constant number of particles, pressure and temperature. For future reference, any XYZ dynamics implies constant X, Y and Z properties.

and Compass force fields. A similar comparison between the experimental and simulated crystal data is presented in Table 2.3. Although the density of the simulated crystal structure was closer to the experimental value with the Compass force field, the cell parameters were in better agreement for the Dreiding force field, which indicated that the orthorhombic nature of the iPMMA crystal was better retained in the latter force field. Furthermore, the density of the crystal was (approximately) only 3% higher with the Dreiding force field, which implied that the Dreiding force field described the interactions in iPMMA in the best manner; it was, therefore, selected to represent the amorphous PMMA. The definitions of each of the energy terms for the Dreiding force fields used in the present study are listed in Appendix D. Van der Waal's interactions are represented by the exponential 6-form as in the original paper (Mayo *et al.*, 1990).

Table 2.2: Comparison of isotactic PMMA crystal data with experimental data after energy minimization.

	Cell Parameters				Density g/ cm^3
	a (Å)	b (Å)	c (Å)	$\alpha = \beta = \gamma$	
Experimental data	41.96	24.34	10.50	90°	1.210
Universal force field	44.31	23.66	11.06	90°	1.147
Dreiding force field	43.65	23.65	10.63	90°	1.210
COMPASS force field	43.88	24.05	10.29	90°	1.220

Table 2.3: Comparison of isotactic PMMA crystal data with experimental data after NPT dynamics.

	Cell Parameters						Density g/ cm^3
	a (Å)	b (Å)	c (Å)	α	β	γ	
Experimental data	41.96	24.34	10.50	90°	90°	90°	1.210
Dreiding force field	42.16	23.69	10.70	90.99°	90.36°	89.18°	1.245
COMPASS force field	46.29	24.63	10.51	89.32°	115.29°	89.81°	1.227

2.3.2 Amorphous PMMA Samples: Building and Optimization

Ideally computations extend over very large and very many molecules in suitably constructed interactive modes, so as to average the computations over a realistically large space domain. However, limitations of computer memory and speed still thwart such a general desire and one is forced to be satisfied with relatively small samples. To enlarge the spatial averaging scale one may, as a substitute, construct a (larger) number of size-feasible molecule samples (models), and then average the response over these separate constructs with the expectation that they represent a reasonable average for a larger molecular model. In a trade-off between model construction time and statistical numbers of models, we chose to construct five distinctly different PMMA samples for averaging purposes.

All samples of amorphous PMMA contained 2256 atoms. Each one consisted of three polymer chains with fifty monomer units per chain. The bulk amorphous state was simulated by use of periodic boundary conditions; the polymer chains were packed into a unit cell and the cell was repeated in three dimensions. Each cell was therefore

surrounded by 26 similar cells as nearest neighbors and if a portion of the chain exited the cell, it reentered the cell from the opposite surface. In effect, an infinitely periodic structure was created. Prior to building these samples, the charges shown in Table 2.1 were transferred to the monomer of PMMA. A typical sample of amorphous PMMA is shown in figure 2.3. The samples were constructed using the amorphous builder module available in Cerius2, a molecular modeling software program.[17]

One of the important issues concerning amorphous polymers is the wide range of spatial conformations available to the polymer chains. These different possibilities were controlled, to some degree, via the two most important parameters affecting the sample configurations, namely, the backbone dihedral angles, which determines the orientation of different bonds with respect to each other, and the initial density which determines the chain packing in the unit cell.

To construct PMMA samples as correctly as possible in a reasonable time frame, the polymer chains were generated by randomly assigning the backbone dihedral angles via the Monte Carlo method.[18] As demonstrated by Fan *et al.* (1994), random assignment of backbone dihedral angles followed by multiple cycles of energy minimization and molecular dynamics, produce similar results in generating polymer chains that are energetically as favorable as those obtained by the conventional method.[19]

The initial density determines the packing of polymer chains in the unit cell and its neighbors, but restricts the conformational space spanned by each polymer chain. By

---

[17] Release 2.0, 1995, developed by Molecular Simulations Inc., 9685 Scranton Rd., San Diego, CA 92121-3752

[18] Prior to energy minimization.

[19] The conventional method for generation of polymer chains consists of a combination of the rotational isomeric state (RIS) model and the Monte Carlo method. However, this procedure is very time consuming.

specifying different initial densities and randomly assigning the backbone dihedral angles for each sample, the overall chain conformation attained in each sample is quite different. The samples assembled in this manner were, therefore, judged to offer better statistically variant representations of the amorphous polymer.

The densities specified were approximately 5 to 10% higher than the desired and experimental value of 1.18 g/cc at 300 K.[20] These initial densities were achieved in three steps. Each sample was built starting at a density of approximately 0.8 g/cc. Lower density allowed the faster construction of the samples. The samples were then subjected to an energy minimization cycle. That was followed by a "temperature annealing cycle" involving NVT dynamics for a short duration (~ 5ps) at 600 K by keeping the cell dimensions fixed. Temperature annealing was necessary to prevent the system from getting trapped in a meta-stable, high-energy but "local" minimum. The sample density was increased by reducing the lengths of the unit cell and coupled with intermediate energy minimization at each step. This procedure was repeated until the initial target density was achieved for each sample.[21] Once the targeted initial density values were achieved, the samples were again subjected to energy minimization, with the cell parameters (a, b, c, α, β, γ) allowed to vary during this process.

---

[20] The initial densities specified are 5-10% higher than experimental density so that after performing full optimization, the final densities achieved for the samples are closer to the experimental density.

[21] Prior experience with Polystyrene (PS) modeling, for which the target initial density was specified directly followed by energy minimization and temperature annealing cycles, revealed that if samples are not properly equilibrated during the building process, jumps in sample density may be observed while performing NPT dynamics. It could be especially true for the polymer chains with large side groups. Therefore, the method specified above was adopted for PMMA sample building.

The initial and final values of densities for each sample are listed in Table 2.4. Ideally, the densities of the final structure should match the experimental values and be independent of their initial densities. However, due to the difference in the overall chain conformations of each sample and different initial densities, a variation in the final values of densities is observed. A comparison of the potential energies of each sample, also listed in Table 2.4, indicates similar values, which illustrates the effectiveness of the building procedure. The average value of the density obtained for the simulated structures is 1.16 g/cc with a standard deviation of 0.035 g/cc.

Table 2.4: Initial densities, final densities, and potential energies of five PMMA samples at 0 K.

Sample	Initial Density (g/cm^3)	Final Density (g/cm^3)	Potential Energy (kcal/ mol)
1	1.29	1.189	10132.87
2	1.22	1.133	10085.96
3	1.25	1.169	10089.72
4	1.27	1.117	10188.72
5	1.30	1.198	10092.14
average		1.162	10117.88
std. deviation		0.035	43.92

The simulated structures must satisfy the criterion that the values of the internal stresses must be (close to) zero, which is equivalent to the structure being at a local minimum of the potential energy surface and assures thus an equilibrium state. The

components of the internal stress tensor are defined as the first derivatives of the potential energy per unit volume with respect to strains.

$$\sigma_{ij} = \frac{1}{V}\frac{\partial E}{\partial \varepsilon_{ij}}$$

where E is the potential energy, ε_{ij} is the component of the strain tensor, and V is the volume of the system. The first derivative of the potential energy, the internal stress tensor at 0 K, with zero kinetic energy associated with atoms, is calculated by summing all forces acting between every pair of atoms.

$$\sigma_{ij} = \frac{1}{2V}\sum_{k\neq l}^{N}\left(r_i^k F_j^{kl} + r_i^l F_j^{lk}\right) = \frac{1}{2V}\sum_{k\neq l}^{N}\left(r_i^k - r_i^l\right) F_j^{kl}$$

where r_i^k is the i^{th} coordinate of atom k and F_j^{kl} is the j^{th} component of the interaction force between the k^{th} and l^{th} atoms. Table 2.5 shows the values of different stress components obtained by averaging over five the samples of PMMA. The values of the stress components clearly indicate that the polymer chains are mechanically relaxed. This criterion usually cannot be satisfied if the density of the simulated structure is fixed by not allowing the cell parameters to vary. The average cell parameters for the five simulated structures are listed in Table 2.6. The deviations in cell lengths and angles are small even though full cell optimizations were performed.[22]

Table 2.5: Average internal stress components (MPa) of five PMMA samples at 0 K.

xx	0.367 ± 0.35	yz	0.178 ± 0.45
yy	0.674 ± 0.73	xz	0.230 ± 0.25
zz	0.912 ± 0.98	xy	0.244 ± 0.20

[22] In addition to the atomic coordinates, the shape of the cell was free to change.

Table 2.6: Average cell parameters of five PMMA samples at 0 K.

a (Å)	27.35 ± 0.52	α (degees)	89.98 ± 0.73
b (Å)	28.12 ± 0.75	β (degrees)	91.22 ± 1.86
c (Å)	27.98 ± 0.62	γ (degrees)	89.81 ± 2.42

The fundamental difference between a crystalline and an amorphous structure is the existence of long-range order in the former and its absence in the latter. The total pair distribution function, g(r), which gives a measure of the spatial organization of atoms about a central atom, can be used to demonstrate the long-range order in a structure. Therefore, the function g(r) can be utilized to distinguish between an amorphous and a crystalline structure. With this in mind, figure 2.4 (a) and (b) present g(r) for the simulated samples and isotactic PMMA crystals, respectively. The peaks of g(r) are an indication of presence of definite correlation between atoms within that radius. A comparison between figures 2.4 (a), which represents the amorphous structure, and (b), corresponding to the crystalline form, clearly demonstrates the difference in the nature of the two structures. The absence of any peaks beyond a 4 Å distance in figure 2.4 (a) indicates that there is no long-range order in the samples. The peaks observed at distances less than 4 Å can be assigned to the specific distances of closely coupled atoms. This spatial distribution function represents thus a completely randomized structure under the constraint on the cell size. In contrast, figure 2.4 (b) indicates the presence of peaks over much greater distances (approximately 8 Å), which implies the existence of a longer range order in the structure.

2.3.3 Simulation Details

Molecular dynamics simulations compute the motions of individual atoms in the system under the influence of the force fields and the surrounding environment. These motions are calculated via finite difference integration of the governing differential equations. One of the main objectives of equilibrium molecular dynamics is to determine the thermodynamic equilibrium properties of a system. If a microscopic dynamic variable, A, evolves in time as a function A(t), then the equilibrium value of A is computed by time averaging as shown in equation (2.1) (Haile, 1997).

$$A_{equi} = \lim_{T\to\infty} \frac{1}{T} \int_0^{\infty} A(t)\,dt \qquad \text{——————————} (2.1)$$

This dynamic variable can be any function of the atomic coordinates and momenta. Several forms of molecular dynamics are available, such as, NVT, NVE, etc. Appropriate forms of molecular dynamics need to be selected to compute the system properties of interest.

The goal of the present study was to determine the bulk compressibility of PMMA as a function of temperature. This was achieved by computing pressure-volume-temperature (PVT) data using NPT dynamics. The bulk compressibility was then calculated from

$$K_T = -\frac{1}{v}\frac{\partial v}{\partial P}\bigg|_T \qquad \text{or} \qquad K_T = \frac{1}{\rho}\frac{\partial \rho}{\partial P}\bigg|_T \qquad \text{——————} (2.2)$$

The formulation of NPT dynamics was based on the work of Andersen (1980) and of Parrinello and Rahman (1980, 1981, and 1982). The Hoover method (1985) was used

to specify the thermal coupling between the system and the heat bath; the thermal relaxation time, which dictates the coupling strength of the system to the heat bath, was set at 0.1 ps. The NPT molecular dynamics equations of motion dynamically control the system temperature and pressure at the specified values of external temperature and pressure. Thus the system was maintained under isobaric conditions with a specified temperature. To accomplish this simulation, the cell dimensions represented by a matrix "h," is introduced as a dynamical variable. To obtain a dynamical equation of motion for h variable, a "cell mass" parameter W is introduced, which may be viewed as representing the inertia of the system and determining the dynamic response of the system. Its value was chosen as 5% of the total mass of the atoms in the unit cell. This particular value was selected to ensure that the system equilibrates quickly and yields sufficient number of oscillations in volume during the course of simulation in order to obtain convergence in density and cell parameters without unnecessarily large fluctuations.

The pressures considered were 0.0001 GPa (atmospheric pressure), 0.25, 0.5 and 1.0 GPa and the temperatures ranged from zero to 500 K, which encompasses the glass transition temperature of PMMA, T_g = 378 K. The simulations were carried out at the specified pressure starting at 100 K and progressively increasing the temperature to 500 K in 100 K increments. The duration of a typical dynamic run was for 25 ps with an integration time step Δt of one femto-second. The first 10 ps of the simulations were approximately necessary to attain mechanical and thermal equilibrium; the final value of the density (or specific volume) at the specified pressure and temperature was obtained by averaging the density data over the remaining 15 ps. The system usually achieved

equilibrium in first 5 ps; however, an additional 5 ps were allowed to ensure equilibrium in every case. Figure 2.5 shows the typical fluctuations in pressure, density and temperature data. One observes that the system quickly equilibrates in less than 5 ps and then continues to fluctuate around the equilibrium value.

2.4 Results and Discussion

We next record the results obtained from experiments and from the simulations. We then present a comparison between the two data sets, which is followed by a discussion of the comparative study.

2.4.1 Results from Experiments

The dynamic bulk compliance of PMMA was determined at atmospheric pressure over a wide range of temperatures and frequencies. The measurements were carried out on irregularly shaped pellets ranging in weight from 0.1 to 0.3 gram, which were purchased from ACE Company (ACE, now a part of Ono). The glass transition temperature was quoted by the manufacturer as 105 ^{o}C.[23] The experimental technique used for measuring dynamic bulk compliance followed McKinney and Belcher's work (McKinney and Belcher, 1963) and employed also in the more recent studies of Deng and Knauss (1997). It employs a small cavity in a (nearly) rigid solid containing the polymer specimen, a non-conductive, pressurizing fluid and two piezoelectric transducers, one serving as a volume expander and the other as a pressure sensor. A sinusoidal voltage applied to one transducer causes commensurate time-dependent pressure variations, which then interact

[23] Simulation computations of the glass transition temperature were also carried out. Appendix E provides more detail on this effort.

with the second piezoelectric element (pressure sensor). The lengths of the stress waves associated with the applied frequencies are much larger than any of the cavity dimensions, so that the (volumetric) deformation of the sample in the cavity occurs under essentially quasi-static hydrostatic pressure. An experimental apparatus along with relevant electronic circuitry was developed in our laboratory by Deng and Knauss (1997). It served as the basic equipment for the measurements on PMMA with modifications in several aspects to make it suitable for measurements at suitable temperatures. For more details on the experimental setup and measurements, the reader is encouraged to refer to Sane and Knauss (2000). Here we present only a summary of the results.

Measurements were made at temperatures between 27° to 123 °C on multiple samples and averaged for determining the dynamic bulk compliance. The storage and loss compliance over the frequency range of 10-1000 Hz is shown in figure 2.6. The measurements were quite repeatable for temperatures below 71 °C; however, uncertainties in the measurements increased up to ± 5 or 6% as temperatures approached the glass transition temperature. The maximum values of uncertainties were observed at high temperatures and low frequencies. The major transition of the storage compliance occurs at temperatures between 81° and 123 °C. Beyond 123 °C, PMMA is expected to approach the bulk rubbery domain.[24] At temperatures below 40 °C the bulk compliance changes more slowly with frequency than at the higher temperatures, and the loss compliance remains virtually constant; this represents the glassy domain.

[24] The current experimental set-up does not allow making reliable measurements beyond 123 °C due to the beginning of thermal degradation of the pressure transmitting oil.

The experimental data was shifted using the time-temperature superposition principle to obtain a master curve, shown in figure 2.7, relative to 105 °C. Both storage and loss compliance data were shifted by identical amounts. For later reference, the corresponding shift factors are shown in figure 2.8. It was observed that the bulk compliance data shifted well for temperatures below 92 °C. However, beyond this temperature the curvatures of both the storage and loss compliance data did not match very well into a master curve, and it was therefore not reasonable to assign a degree of reliability to the shifted data in the high temperature range.

2.4.2 Simulation Results

To explore the effect of loading history on the bulk compressibility, two types of loading conditions were considered in the NPT dynamics simulations on the amorphous PMMA. In the first case, the external pressure was increased from 0.0001 to 1.0 GPa (loading conditions) and as a second case, pressure loading was decreased from 1.0 to 0.0001 GPa (unloading conditions) for each temperature. Simulations were carried out on the three samples and averaged. Figures 2.9 and 2.10 show the pressure variation of the density along an isotherm for loading and unloading conditions, and Table 2.7 lists the values of densities obtained at each pressure and temperature. From that table one gages the effect of loading history (loading vis-à-vis unloading) on the values of densities disappears at "high" pressures (approximately beyond 0.25 GPa), the difference in densities being generally less than 0.5%. However, near atmospheric pressures this difference is tangible. For example, at atmospheric pressure and 300 K, it is approximately 5%. More importantly, the slope of the isotherms, which according to equation 2.2 effect the bulk compressibility, are substantially different under loading and unloading conditions for

lower pressures. Thus, to determine the bulk compressibility accurately at lower pressures, it is essential to determine the slopes of the isotherms carefully.

Table 2.7: Densities under loading and unloading conditions.

Pressure	Loading conditions					Unloading conditions				
GPa	100 K	200 K	300 K	400 K	500 K	100 K	200 K	300 K	400 K	500 K
0.0001	1.144	1.133	1.109	1.098	1.098	1.196	1.177	1.161	1.149	1.144
0.2500	1.231	1.222	1.218	1.204	1.194	1.233	1.221	1.206	1.196	1.192
0.5000	1.274	1.268	1.256	1.246	1.237	1.271	1.265	1.251	1.243	1.240
1.0000	1.343	1.337	1.333	1.322	1.310	1.340	1.327	1.328	1.323	1.303

The differences in the densities and the slopes of the isotherms near atmospheric pressures (loading vis-à-vis unloading) is probably a feature of the modeling process rather than a physical phenomenon exemplifying permanent compressibility or yielding. To explore this model-conditioned behavior further, each model sample was first subjected to the loading cycle followed by an unloading cycle. After passing through this loading cycle, the polymer chains in the samples did not regain their original configurations and resulted essentially in squeezing out the excess volume present in the samples. The thermal cycling of the samples (i.e., going from zero to 500 K and back to zero K) further augmented the configurational changes in the samples; the polymer chains were able to sample different conformational spaces, which led to different local energy minima. From Table 2.8, one observes that there is a better agreement of the properties

such as density and coefficient of thermal expansion between the experimental measurements and the results obtained from unloading case than as compared with the loading case. Furthermore, when the samples were loaded again (i.e., pressure increased from 0.0001 to 1.0 GPa) after being subjected to a complete loading-unloading cycle, the variation of density with pressure for each temperature followed almost the same path as obtained during the previous unloading conditions (the difference in densities obtained from unloading and reloading was less than 1%) as demonstrated in figure 2.11 for a particular case of 300 K. Thus one can infer that the initial loading (from 0.0001 to 1.0 GPa) of the samples should be considered as a part of sample conditioning (equilibration) process similar to temperature annealing cycles as mentioned in Section 2.3.

Table 2.8: Comparison of properties (density and coefficient of thermal expansion) at atmospheric pressure and 300 K between experimental results and those obtained under loading and unloading cases for amorphous PMMA.

	Density (g/cc)	Coefficient of thermal expansion /K	
		Below T_g	Above T_g
Experiments*	1.18	2.53×10^{-4}	5.74×10^{-4}
loading	1.11	1.00×10^{-4}	3.00×10^{-5}
unloading	1.16	1.00×10^{-4}	3.00×10^{-4}

*Experimental results were taken from Polymer Handbook (1989). Average values of PMMA were considered for comparison.

In this context a comment is in order with respect to the sample conditioning during the construction phase. Recall that a part of the building process consisted of consolidation following an initial choice of the density. The pressurization histories described in this section provide, in principle, the same effect, except that larger consolidation pressures are incurred than those employed initially. This observation demonstrates clearly that the initial building process was insufficient to establish an energy-minimized equilibrium structure, but that higher pressure excursions are needed than might normally be surmised to arrive at an equilibrium model. With this understanding, we limit evaluations of the NPT data to the unloading portion of the pressure histories.

Based on the set of pressure-density-temperature data as obtained from the unloading histories, the isothermal bulk compliance of PMMA was calculated as a function of temperature using equation 2.2. To compare the simulation results, excerpts from the laboratory measurements were selected as a function of temperature and at the single frequency of one kHz. That comparison between the simulations and the experimental results is shown in figure 2.12. Tables 2.9 and 2.10 list the bulk compliance values obtained from the computations and the measurements at one kHz at different temperatures. In figure 2.12 we have also included the bulk compressibility as computed from the PVT data for the initial loading conditions. The difference in the bulk compliance values obtained from this initial loading and from the unloading history amounts to approximately a factor of two. In view of the fact that the magnitude of the bulk compliance changes by only a small factor of two or three throughout the viscoelastic transition, this difference in the computed bulk compliance is substantial and

it appears, therefore, essential to condition the samples through a loading cycle prior to performing any computations.

Table 2.9: Bulk compliance $(GPa)^{-1}$, as a function of temperature from the simulations at atmospheric pressure.

Temperature (K)	Loading condition	Unloading condition
100	0.371	0.130
200	0.416	0.172
300	0.443	0.168
400	0.462	0.173
500	0.478	0.194

Table 2.10: Bulk compliance $(GPa)^{-1}$, as a function of temperature from the experimental results at 1 kHz at atmospheric pressure.

Temperature (K)	Bulk compliance at 1 kHz
300.54	0.169
311.71	0.169
322.40	0.184
333.34	0.183
344.15	0.199
354.88	0.244
365.20	0.257
375.54	0.287
385.96	0.292
396.01	0.311

Discounting the unreasonable effects derived from the initial loading history, the computations demonstrate the correct order of magnitude for the bulk compliance. However, the variation of the bulk compliance observed in the experimental data with temperature is much more pronounced than the computations indicate. This was expected because the computations provide information on the bulk behavior at very high frequencies on the order of giga hertz (or very small time scales on the order of nano-seconds) and only a small variation in the bulk compliance was observed over a temperature range of 100 to 500 K. In the full documentation of the measurements Sane and Knauss (2000) make a plausible argument, based on the (tentative) use of the time-temperature superposition principle, that the variation of the simulated compliance should not be significant over the temperature range considered. In contrast, the measurements reveal significant variations of the compliance of PMMA in the frequency range of 10-1000 Hz (in the milli-seconds time scale), and therefore over this frequency range the "glass-to-rubber" transition was observed a temperature range of 300 to 430 K.

Another important issue deserving attention regards the modeling of the bulk compliance. It is often believed that the molecular mechanisms controlling bulk deformations depend only on very local motions of the polymer molecules and that long range entanglements (and cross-links) play no or a subsidiary role. In contrast, the shear behavior is supposed to be governed by local as well as long range molecular interactions and rearrangements. Therefore, it was believed that due of the presence of dominant local interactions in bulk behavior, predicting the bulk behavior for polymers using molecular modeling techniques would be relatively simpler and more accurate than predicting the shear behavior. However, in figure 2.8, the master curves corresponding of the bulk

response data illustrate that the range of the bulk transition is extended over about eight decades of time or frequency, which is comparable to the transition range of the shear response (Sane and Knauss, 2000), which indicates that the molecular mechanisms controlling the bulk deformations may not just involve very local interactions.

It has been suggested that the molecular contributions to the bulk deformations in PMMA could be derived primarily from the motion of the ester side groups, which are relatively massive, coupled with the motion of the chain backbone, with, however, the rotations and oscillations of the side groups playing a dominant role. These molecular motions governing the bulk response are still relatively short-ranged as compared to medium and long-range interactions present in shear behavior. While the measure of "short-range interactions" is debatable, the current study certainly raises the question of "sufficiency" in terms of molecular modeling of polymers. The amorphous PMMA samples in the present study contained three polymer chains with 50 monomer units in each. Even though the current 2256 atom samples can be considered as fairly large, one needs to address the issue of whether these models were able to represent all the possible molecular interactions present in bulk deformations, especially those concerning the coupling of the ester side group with the chain backbone and its impact on the overall chain dynamics. One also needs to explore the effects of number of polymer chains present in a model on the final results of bulk compliance. With the current composition of the PMMA samples, molecular dynamics simulations were able to compute the thermodynamic properties such as density and coefficient of thermal expansion with a fair degree of accuracy, however, in order to predict more complex properties such as time

dependent bulk or shear response of amorphous polymers, further modeling refinements are needed.

2.5 Concluding Remarks

Models of amorphous PMMA were constructed to study the bulk compliance as a function of temperature. The Dreiding force field was used to describe the interactions in amorphous PMMA, it having been selected through a comparative study on isotactic PMMA crystals for which X-ray structural analysis data was available. The models of amorphous PMMA were subjected to NPT dynamics, i.e., constant number of particles, pressure, and temperature, to determine the pressure-volume (or density)-temperature data. The effect of loading history on the samples was studied by first loading (external pressure increasing) and then unloading (external pressure decreasing) the samples. Significant differences in densities were observed near atmospheric pressures between the initial loading and unloading histories. The initial loading of the samples was, therefore, considered as a sample conditioning (equilibration) process, an essential procedure to be accounted for in modeling to derive accurate results. Based on the PVT data for unloading histories, the isothermal bulk compliance was computed as a function of temperature. A comparison with the experimental results revealed a better agreement with the computed data near room temperature. However, the simulations were not able to capture the variation of the bulk compliance with temperature, completely. On the other hand, good agreement between the experimental and computed values of density and glassy coefficient of thermal expansion was observed.

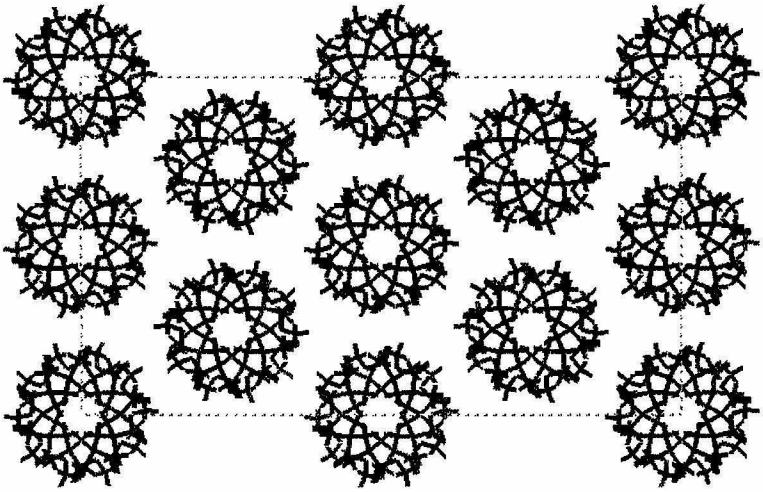

Figure 2.1: Crystal Structure of Isotactic PMMA.

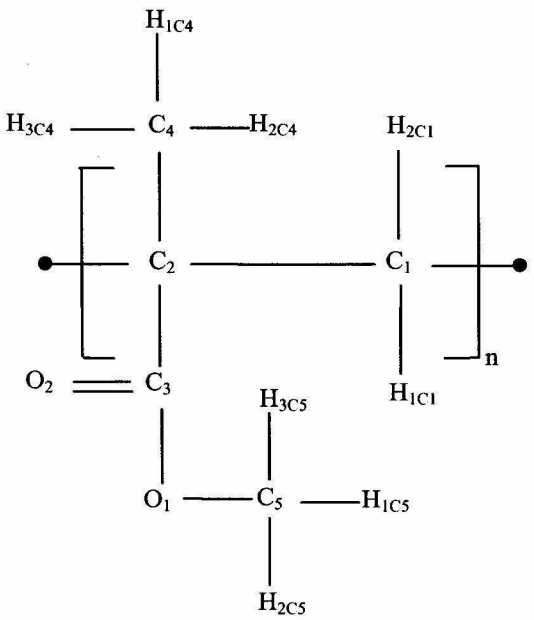

Figure 2.2: PMMA monomer.

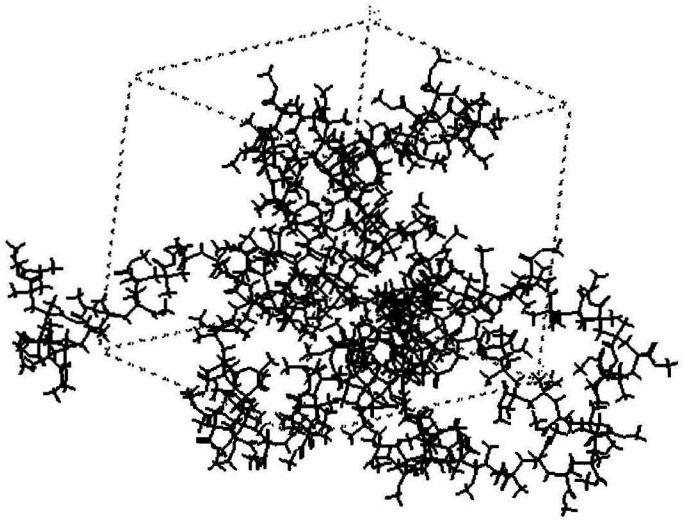

Figure 2.3: Amorphous PMMA model.

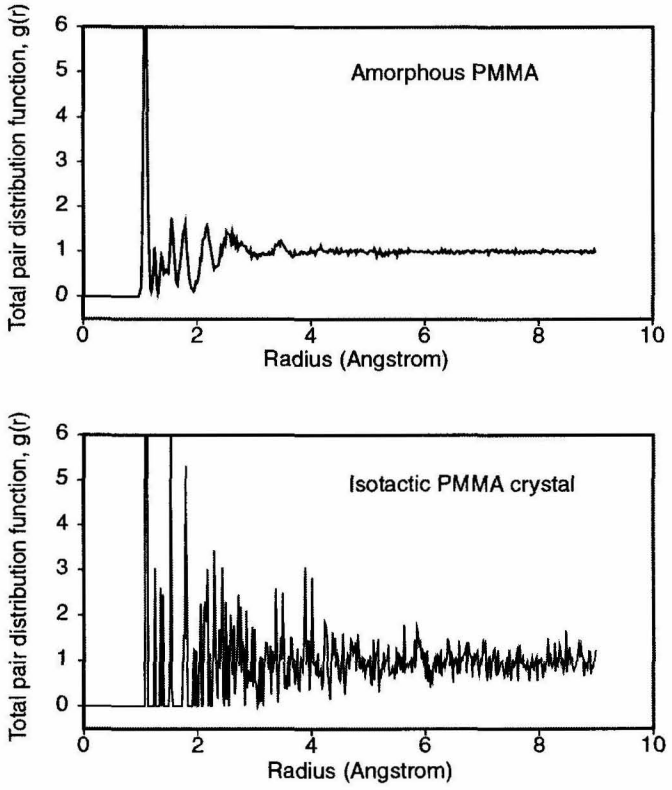

Figure 2.4: Total pair distribution function, g(r); a) for model PMMA sample and b) Isotactic PMMA crystal.

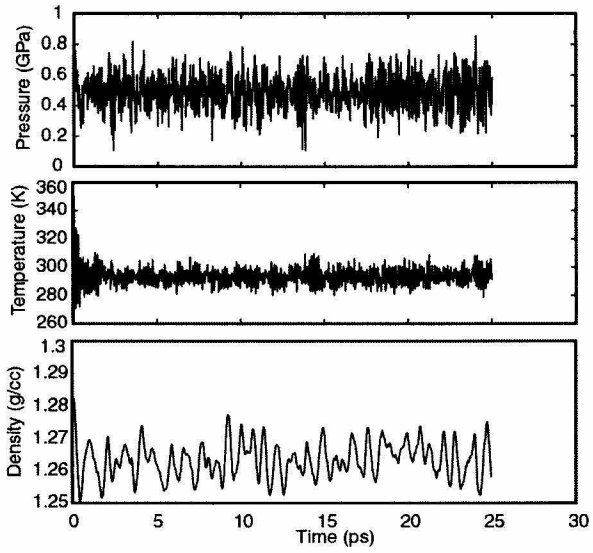

Figure 2.5: Typical fluctuations of pressure, temperature and density during NPT dynamics. A particular case is shown for a specified external pressure of 0.5 GPa and temperature of 300 K.

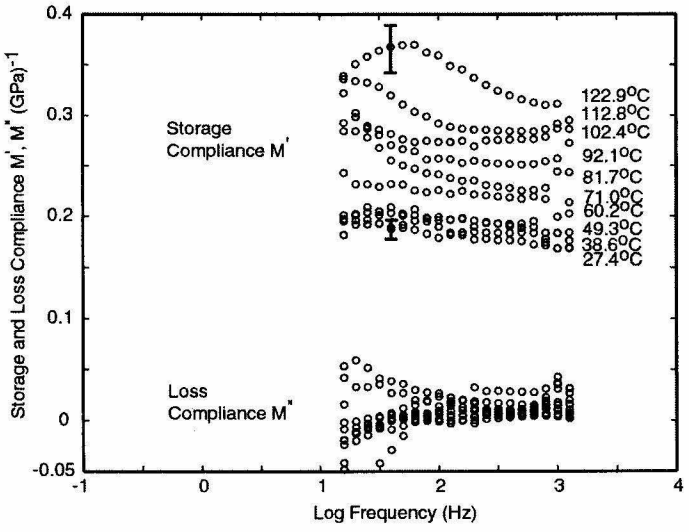

Figure 2.6: Storage M′ and loss compliance M″ of PMMA at indicated temperatures over two decades of frequency. Note error bar estimates at extreme temperatures.

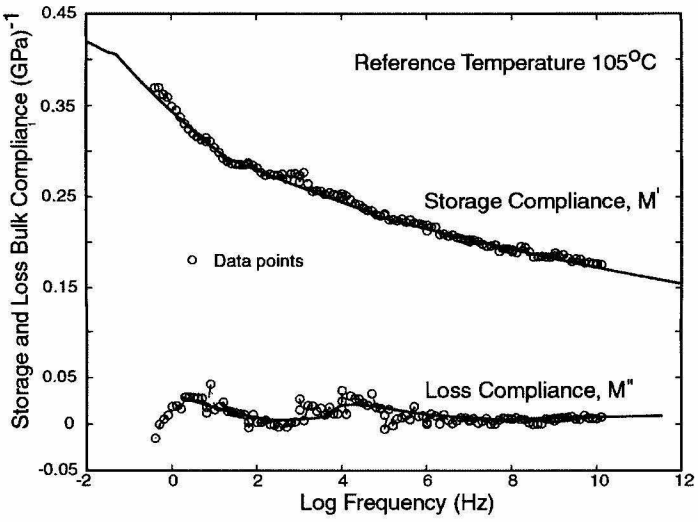

Figure 2.7: Master curves of storage and loss bulk compliances for PMMA at a reference temperature of 105 °C.

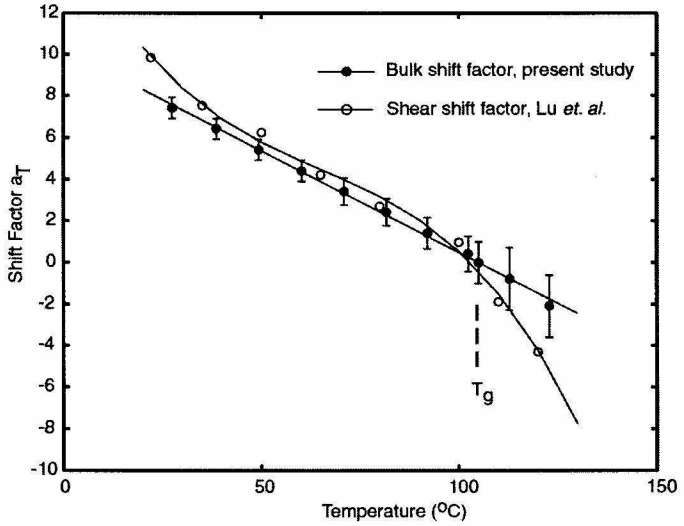

Figure 2.8: Comparison of the shift factors for the bulk compliance of PMMA with that for the shear compliance (Lu *et al.*, 1997).

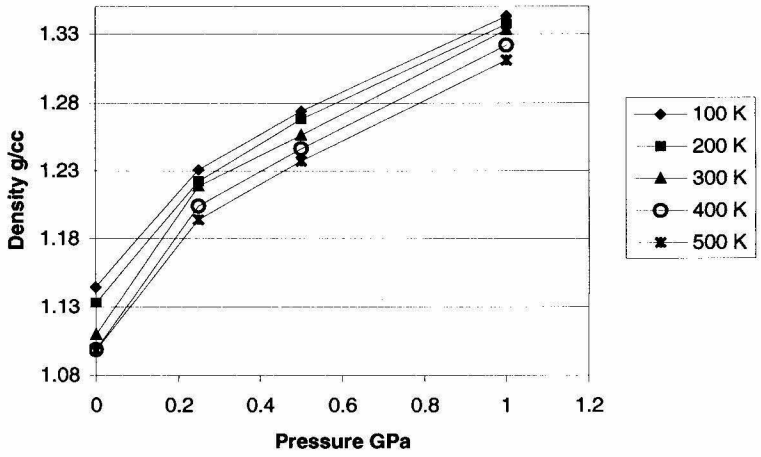

Figure 2.9: Variation of density with pressure along isotherms, under loading conditions; pressure was increased from 0.0001 to 1.0 GPa for each temperature.

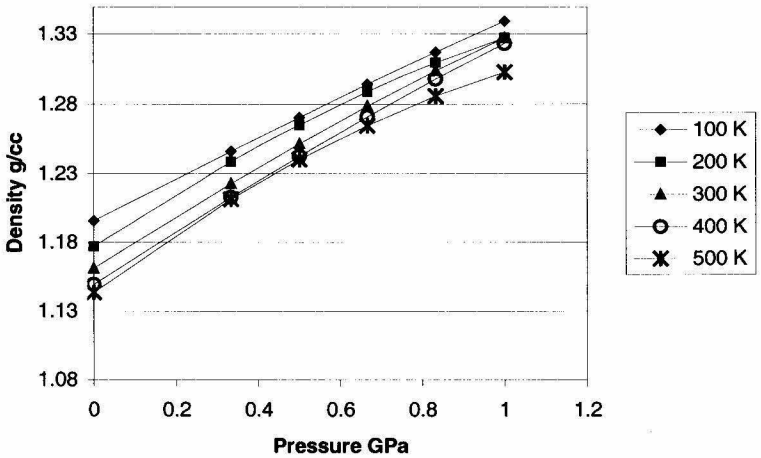

Figure 2.10: Variation of density with pressure along isotherms, under unloading conditions; pressure was decreased from 1.0 to 0.0001 GPa for each temperature.

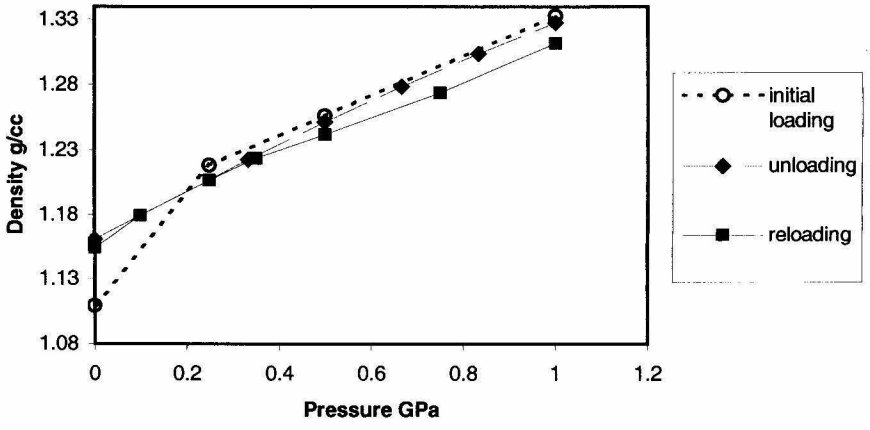

Figure 2.11: An example of reloading the PMMA sample at 300 K after being subjected to one loading-unloading cycle. The difference in densities is less than a percent between unloading and reloading conditions.

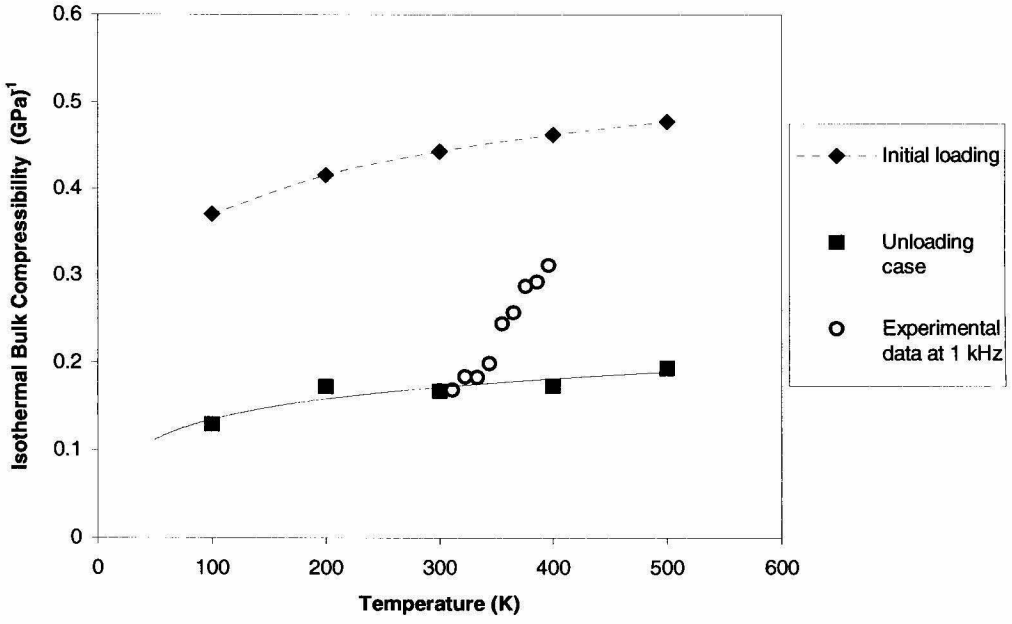

Figure 2.12: Comparison of bulk compliance of PMMA; a) data derived from PVT data obtained from initial loading conditions, b) experimental results at 1 kHz reported by Sane and Knauss (2000), c) data derived form PVT data obtained from unloading conditions.

Chapter 3

On Interconversion of Various Material Functions of PMMA

3.1 Introduction

The phenomenological theory of (linear) viscoelasticity establishes a complete set of material functions to describe the constitutive behavior of a certain class of materials. Though rather widely recognized for representation of various materials, it is mostly applied in the context of the small deformations of polymers. For isotropic media the theory asserts that, in principle, only two independent material functions need to be measured, from which all others can be computed unequivocally, whether in the typical time or frequency domains. Any two of the linear viscoelastic functions for each mode of loading or deformations (i.e., shear, bulk or uniaxial) contain essentially the same information on the time (or frequency) dependent behavior of the material and, in principle, are equivalent. As a consequence, use has been made of convertibility, typically when one type of property was needed, though not directly available or measurable, but when it could be computed (inverted) with or without an assumption regarding another property (*e.g.*, Poisson's ratio = ½, or time-independent bulk properties). The material function typically missing was either the bulk modulus or compliance, or the Poisson function, with shear or uniaxial material representation being the most common means of material characterization. The unique "interconversion" of properties has been documented for decades and, therefore, it should be possible to compute the bulk (dilatational) response or Poisson behavior from shear and uniaxial data, but this has

proven realistically not possible (Lu *et al.,* 1997). The main reason is the exceedingly high precision required of the measurements to deliver the whole time or frequency range of the desired functions.

Although the mathematical basis for such interconversion between various material functions has been long established, there have been only a few attempts to compare direct experimental measurement with the corresponding material functions obtained by means of computation from other functions. For example, Yee and Takemori (1982) have demonstrated a comparison between the shear modulus obtained from the direct measurements with the computed data from uniaxial and Poisson's data. Unfortunately, in the literature there is a dearth of such comparisons mainly due to the lack of reliable information on all the four time-dependent material functions for the same material.

One may question, of course, whether such a comparison is at all necessary, since the mathematical framework is well established. The primary reasons for performing such a comparison is not a check on the mathematics, though the precision of the interconversion may be in question, but a check on the precision with which the properties need to be determined experimentally. While the error of individual measurements can be typically estimated, the material functions are, usually, determined with the aid of the time-temperature superposition principle. This principle is applied to data acquired over a limited range of time scales and the quality of its applicability is normally judged by how well shifted data segments overlap. This judgment depends heavily on the curvature of the data segments, which can be increased only by performing measurements over extended periods of time or large ranges of frequency. However, in this regard equipment usually imposes limitations through structural resonance (dynamic

measurements) or, typically[25], by loss of electronic stability or drift when creep or relaxation measurements are made. Thus, when data has been acquired by time-temperature superposition, a computational interconversion and data comparison with experiment ultimately tests the quality of the shift procedure, or, in fact, the applicability of that process itself. It is thus our intent to examine these issues in the framework of normal and relatively careful engineering measurements.

A quick literature search would reveal that there is an abundance of measurements on shear and (mostly) uniaxial behavior of various polymers, but with very few measurements of a Poisson function, the latter behavior being usually characterized by a constant in either the glassy or near-rubbery domains. However, very little information is available on the time-dependent bulk or Poisson's response of these polymers. Having been concerned with this topic for some time and having measured these quantities in our laboratory, it is, to our knowledge, thus the first time that four material functions on the same material have become available through experiments (Lu *et al.,* 1997; Sane and Knauss, 2000) over a relatively large, if not complete, time or frequency range, to permit such an examination. During the past several years, various material functions of PMMA were measured, namely, E(t), the relaxation moduli in uniaxial tension and in shear, $\mu(t)$, as well as Poisson's ratio, $\nu(t)$ (Lu *et al.,* 1997). Recent, direct measurements over a wide range of temperatures and frequencies were collected on the dynamic bulk compliance of PMMA, denoted here by $M^*(\omega)$. Excepting the Poisson measurements, the specimens used in all the measurements were taken from the same batch of PMMA.

---

[25] Notable exceptions are the extensive but time consuming measurements by Kubát (1965, 1976, and 1986) and his collaborators.

The paper is organized into a brief account of the experimental circumstances relating to the acquisition for the relevant material functions in Section 3.2, followed by analytical background given in Section 3.3. In Section 3.4, a comparison of computed functions and direct measurements for uniaxial, shear and Poisson's ratio is reported, followed by an examination of possible reasons for observed differences. A summary in Section 3.5 concludes the presentation. The data procured by Yee and Takamori are included in these presentations to the extent that they provide further insight into the precision and interconvertability issue, even though they demonstrate that the PMMA in that study is clearly different from that used in our more recent work. In view of the ultimate result of this investigation concerning the applicability of the time-temperature shift procedure in the present context a caveat is in order, namely that the Yee/Takamori data is incorporated with such shifting to relate it to the proper temperature and time or frequency range of the present data. This representation may not be appropriate.

3.2 Review of Experimental Data

In this section we briefly review details of the measurements carried out in our laboratories to determine the various material functions of PMMA.

3.2.1 Shear, Uniaxial and Poisson Responses

Two sets of material functions in relaxation (uniaxial & Poisson's response; uniaxial & shear response) for PMMA have been reported by Lu *et al.* (1997) over a wide range of temperatures. For the first set, PMMA material was acquired from Rohm & Haas (glass transition temperature of 105 °C) and strip specimens were used to determine the uniaxial modulus and Poisson's ratio in relaxation. Image moire was used to monitor the specimen

deformation with time under strain. In the second set, cast PMMA in cylinder form was purchased from ACE, (now a part of Ono), with the glass transition temperature quoted by the manufacturer as 105 °C. Hollow tubular specimens were machined to separately measure the uniaxial and the shear modulus in relaxation. For these measurements digital image correlation was used to monitor the surface deformations. In both cases, the specimens were annealed by holding them above the glass transition temperature for more than two hours after which they were allowed to cool to room temperature at a rate of approximately 5 °C/hour. Subsequently they were stored at room temperature for several days.

Apart from the Yee/Takamori data, only the Poisson data from the first set is used together with the uniaxial and shear relaxation data from the second set. Figures 3.1, 3.2 and 3.3 illustrate the master curves corresponding to the uniaxial, shear and Poisson's response at a reference temperature of 105 °C.

3.2.2 The Dynamic Bulk Compliance

The dynamic bulk compliance of PMMA was measured at atmospheric pressure over a wide range of temperatures and frequencies. These measurements were carried out on annealed PMMA specimens, which were irregularly shaped pellets ranging in weight from 0.1 to 0.3 gram. The specimens were taken from the same batch as those used by Lu *et al.* The experimental method used for measuring the dynamic bulk compliance was based on the Belcher/McKinney method (McKinney *et al.*, 1956), which has been implemented and refined more recently by Deng and Knauss (1997) and by Sane and Knauss (2000). It employs a small cavity in a (nearly) rigid solid containing the polymer specimen, together with a non-conductive (pressurizing) fluid and two piezoelectric

transducers, one serving as a volume expander and the other as a pressure sensor. A sinusoidal voltage applied to one transducer causes commensurate time-dependent pressure variations, which then interact with the second piezoelectric element (pressure sensor). The lengths of the stress waves associated with the applied frequencies are much larger than any of the cavity dimensions. Under these conditions, the (volumetric) deformation of the sample in the cavity occurs under essentially quasi-static hydrostatic pressure. An experimental apparatus along with relevant electronic circuitry was developed in our laboratory by Deng and Knauss (1997) in connection with their work on PVAc. It served as the starter equipment for the measurements on PMMA, but had to be modified to permit measurements at the higher temperatures required for PMMA. For more details on the experimental setup and measurements, the reader is encouraged to refer to Sane and Knauss (2000). Here we present only those results essential for the current analysis.

Measurements were made over the temperature range from 27° to 123 °C with the frequency ranging from 10 to 1000 Hz. The segments of storage and loss compliance shown in figure 3.4 at different temperatures were shifted according to the time-temperature superposition principle to obtain master curves. Figure 3.5 shows the resulting (storage and loss) master curves relative to 105 °C. The measurements were quite repeatable for temperatures below 71 °C; however, uncertainties increased up to ± 5 or 6% as temperatures approached the glass transition temperature. The maximum values of uncertainties were observed at high temperatures and low frequencies. The major transition of the storage compliance occurs at temperatures between 81° and 123 °C.

Beyond 123 °C, PMMA is expected to approach the bulk rubbery domain.[26] At temperatures below 40 °C the bulk compliance changes more slowly with frequency than at the higher temperatures, and the loss compliance remains virtually constant; this represents the glassy domain.

3.3 Analytical Background

We next consider the procedure and relevant formulae of interconversion. The data on uniaxial (E(t)), shear ($\mu(t)$) and Poisson's ($\nu(t)$) response on PMMA was available as functions of time, while the dynamic bulk compliance $M^*(\omega)$ was obtained as a function of frequency. To examine interconversion among various material functions, the relaxation data, i.e., E(t), $\mu(t)$, and $\nu(t)$ approximately, were first Fourier transformed to yield corresponding dynamic viscoelastic functions

$$\begin{aligned} E^*(\omega) &= (i\omega)F\{E(t),t\rightarrow\omega\} = E'(\omega) + i\,E''(\omega) \\ \mu^*(\omega) &= (i\omega)F\{\mu(t),t\rightarrow\omega\} = \mu'(\omega) + i\,\mu''(\omega) \qquad \text{——————(3.1)} \\ M^*(\omega) &= M'(\omega) - i\,M''(\omega) \end{aligned}$$

where $F\{\cdot,t\rightarrow\omega\}$ denotes the Fourier Transform of the function in braces. A 15 term (N = 15) Prony-Dirichlet series (Tschoegl, 1989) of the form

$$w(t) = w_o + \Sigma\, w_i \exp(-t/\tau_i) \qquad \text{——————(3.2)}$$

[26] The current experimental set-up does not allow us to carry out reliable measurements beyond 123 °C due to beginning of thermal degradation of the pressure transmitting oil.

was fitted through the relaxation data E(t) and $\mu(t)$ to effect the computation. The parameters in the equation (3.2), w_i's are the weights associated with the relaxation time τ_i's

The parameters w_i and τ_i were determined using an algorithm developed by Emri and Tschoegl (1993 and 1994). Figures 3.1 and 3.2 illustrate a good fit of the Prony series representation to the experimental uniaxial and shear data. The dynamic moduli were then computed as indicated in equation (3.3) (for more detail refer to Tschoegl, 1989, chapter 8).

$$w^*(f) = w'(f) + j\,w''(f), \quad \text{where } \omega = 2\pi f \;\&\; f = \frac{1}{t}$$

$$w'(f) = w_o + \sum_{i=1}^{N} \frac{w_i (2\pi f \tau_i)^2}{1+(2\pi f \tau_i)^2} \;\&\; w''(f) = \sum_{i=1}^{N} \frac{w_i (2\pi f \tau_i)}{1+(2\pi f \tau_i)^2} \qquad \text{——————(3.3)}$$

The curve of the form in equation (3.4) was fitted through the Poisson data (Lu *et al.*, 1997), as illustrated in figure 3.3.

$$\nu(t) = \nu_i - \left(\frac{\nu_i - \nu_o}{1+(t/\tau)^p} \right) \qquad \text{——————(3.4)}$$

where $\nu_i = 0.5$, $\nu_o = 0.31$, $p = 0.155$, and $\tau = 0.2$

Since this data has been derived from relaxation measurements its Fourier Transform does not represent the Poisson response under cyclical uniaxial straining. However, on physical grounds one expects that in the latter situation the Poisson response renders a low Poisson value for high frequencies and a higher value for low frequencies, with a value close to 0.5 for near-rubbery response. Specifically, the time or frequency response over the range for which the bulk behavior was determined should correspond approximately to the time scale $-10<\log t<0$. This expected trend is, indeed, followed in the Yee/Takamori measurements though not in agreement with the present measurements.

On a heuristic basis, the comparative function has been computed from (3.4) via the approximation[27] suggested by Schapery, as shown in equation (3.5) and by letting $\omega \cong 1/t$.

$$\nu(t) = s\overline{\nu(s)}\Big|_{s=\frac{e^{-c}}{t}} = \nu^*(\omega) \qquad \text{(3.5)}$$

where exp(-c) = 0.56, c is called Euler's constant.

The complex Poisson's function is then represented here through its absolute value. Of interest in the sequel is primarily its amplitude within the frequency range considered rather than its precise dependence on frequency.

Within the realm of linear viscoelasticity, the relationships among the various dynamic material functions are identical to the corresponding relationships amongst their elastic counterparts (except that the former are functions of frequency). Equation (3.6) documents these relationships between E^*, μ^*, ν^* and M^* as used in the sequel.

$$E^* = \frac{9\mu^*}{3 + M^*\mu^*} \qquad \mu^* = \frac{3E^*}{9 - E^*M^*}$$

$$\nu^* = \frac{1}{2}\left(1 - \frac{E^*M^*}{3}\right) \qquad \nu^* = \frac{1}{2}\left(\frac{9}{3 + M^*\mu^*}\right) - 1 \qquad \text{(3.6)}$$

3.4 Results and Discussions

Before effecting the comparisons, which do not render close agreements, it is appropriate to discuss the errors underlying the experimental determination of the material functions.

[27] Due to the non-integer value of "p" in equation 4, when $s \rightarrow i\omega$ in equation 3.5, the function becomes multi-valued. For the present analysis, the principal value of the function $\nu^*(\omega)$ was used.

These errors have then a commensurate effect on the computed (interconverted) material functions.

3.4.1 The Influence of General Data Precision

It is of interest to estimate the errors in the computed functions due the experimental errors underlying the physical data. The relative errors in E* and μ* when computed from [μ*, M*] and [E*, M*], respectively, are

$$\frac{\Delta E^*}{E^*} = \frac{1}{(3+\mu^* M^*)}\left[3\frac{\Delta\mu^*}{\mu^*} + \mu^* M^* \frac{\Delta M^*}{M^*}\right]$$

$$\frac{\Delta \mu^*}{\mu^*} = \frac{1}{9 - E^* M^*}\left[9\frac{\Delta E^*}{E^*} + E^* M^* \frac{\Delta M^*}{M^*}\right] \qquad \text{(3.7 (a))}$$

and in a similar manner errors in Poisson's ratio are given by

$$\frac{\Delta \nu^*}{\nu^*} = \frac{4.5 M^* \mu^*}{\nu^* (3+M^*\mu^*)^2}\left[\frac{\Delta\mu^*}{\mu^*} + \frac{\Delta M^*}{M^*}\right]$$

$$\frac{\Delta \nu^*}{\nu^*} = \frac{E^* M^*}{6\nu^*}\left[\frac{\Delta E^*}{E^*} + \frac{\Delta M^*}{M^*}\right] \qquad \text{(3.7 (b))}$$

For reference we note that the determination of the shear and uniaxial data were, typically, subject to measurement errors of ±3% (Lu *et al.*, 1997). By contrast, the Poisson function, depicted in figure 3.3, incurred larger measurement errors of close to ±6%. Individual Poisson measurements at progressive time intervals possessed an accuracy of about ± 3%; however, when these measurements, obtained at different temperatures, were combined into a master curve, the resulting scatter band yielded a deviation on the order of ± 5 to 6%, depending on whether time-temperature shifting was

accomplished so as to generate a "best" master curve [± 5%], or whether the shifting used the same shift factor as that deduced from shifting the uniaxial relaxation modulus data [± 6 %,][28], these errors are based on a mean Poisson ratio value of 0.4.

The precision of the bulk measurements is similar to that of the Poisson function, though not uniformly so, but increasing from a dominant ± 4% over most of the frequency range to as much as possibly ± 8% at the high-temperature and low-frequency end, where deviations are more pronounced. For later reference it is of interest to note that ultrasonic measurements at room temperature have established a bulk compliance of 0.167 GPa^{-1} (Lu *et al.*, 1997). Although the precise frequency range appropriate for this measurement has not been determined, this value agrees well with that determined by our dynamic method at room temperature and one kHz. This information is of importance in our later discussion on potential errors in the bulk response. With the aid of these values and equations 3.7(a) and (b), one deduces the potential error in the computed values of $E^*(\omega)$, $\mu^*(\omega)$ and $\nu^*(\omega)$ should not be greater than 5%.

3.4.2 Dynamic Uniaxial and Shear Modulus

We turn next to the comparison between the directly measured material functions and their counterparts computed from equation (3.6). All computational results are referred to the glass transition temperature of the polymer (T_g = 105 °C); when the computations depend on the bulk modulus, the frequencies are limited to the range spanned by the dynamic bulk compliance data.

---

[28] The reference (Lu *et al.*; 1997, page 10) contains an error in that it states the error limits for Poisson's ratio as being ± 10%; it should be ± 5% for a full range of 10%.

Using μ^* (figure 3.7) as derived from measurements and M^* (figure 3.5), the dynamic uniaxial modulus, E^*, was computed. Similarly, the dynamic shear modulus, μ^*, was calculated from E^* (figure 3.6) and M^* (figure 3.5). The functions E^* and μ^* so computed are then compared with the corresponding directly measured quantities in figures 3.6 and 3.7. While the overall nature of the converted functions are in agreement with those measured, one observes a substantial and systematic difference in the storage modulus (real part) for both cases. One notes that the loss moduli are in fairly good agreement, but this may be simply the result of their small absolute values, a ten percent error of which is not prominent on the scale of the plot. Figure 3.8 illustrates the numerical deviation between measurements and computations. The relatively small variations around the solid lines are the consequence of the Prony series representation, yet the net differences are, on average, over the frequency range, on the order of 9% (negative) for the uniaxial data and 11% (positive) for the shear data.

3.4.3 Dynamic Poisson's Ratio

The Poisson's ratio ($|\nu^*|$) was calculated from the material functions [μ^*, M^*] and from [E^*, M^*], respectively, with the results shown in figure 3.9. One notes that the overall nature of the computed functions does not even agree qualitatively with the expected amplitude variation of the "measured" data. While the material functions computed from [μ^*, M^*] and [E^*, M^*] predict an essentially constant value for the $|\nu^*|$, and differing by only 2.5% (within experimental error), the "experimental" data shows a monotonically decreasing function with increasing frequency, that is followed functionally, if not numerically, by the Yee/Takamori data.

3.4.4 Possible Reasons for the Discrepancy

We explore next the possible reasons for the differences in the measured and converted functions delineated in Sections 3.4.2 and 3.4.3. We first note that possible sources of experimental errors can derive from material variability and potentially from physical aging; however, these phenomena have been (virtually) eliminated in the experimental phase of the present study (Lu thesis 1997; Lu *et al.*, 1997). Therefore, special attention focuses on potential errors arising from the time-temperature trade-off procedure and on those derived from possibly nonlinear response. In general, it is quite difficult to define the onset of nonlinear material response, and performing measurements at too high a deformation or stress level for ease of instrumentation can readily lead to errors in the 5 to 10% range. Experience in our own laboratory has shown that well below the glass transition temperature nonlinear behavior can readily occur at strain levels from 0.5 to 1% strain. The fact that tensile loading causes accelerated deformations in the nonlinear range can thus have an important, but often unrecognized contribution to the measurements. On the other hand, we shall observe that the expected influence is opposite to the discrepancies observed later on: Under creep conditions one would expect that the creep response should render larger values than linear theory would predict, and under relaxation conditions the stress level (modulus) should be smaller than linear theory would anticipate. Thus, this particular aspect of error source does not seem to play a significant role in the discrepancies noted below.

Turning to the direct comparisons, one observes from figures 3.6 and 3.7 that the difference in the storage compliance is systematic essentially over the whole frequency

range. For reference the data from Yee and Takamori's work are also shown.[29] It is thus natural to inquire whether this is due to a shift along the frequency axis or, alternately, due to a multiplicative factor on the uniaxial or shear functions. To explore the role of variations in time dependence, the bulk compliance curve was shifted by arbitrary amounts to smaller or higher frequencies on a trial-and-error basis. One then finds that to bring the computed and measured functions into closer – though not perfect – agreement, it is necessary to frequency-shift the bulk data by as much as five decades. From the bulk compliance measurements it is clear, however, that the uncertainty in the bulk data due to time-temperature shifting was not consistent with such a large and uniform shift. Consequently, the shift process in and of itself is not likely to account for the disagreement between measurements and computation. As an alternate possible reason for the discrepancy, the error in magnitude of the uniaxial and of the shear data was considered. As one example, the experimentally determined shear modulus function was increased by an amount consistent with the maximum error of ± 3% established for the measurements. The result, shown also in figure 3.6, is reasonably close to the measured function. Similarly, a commensurate decrease in the measured uniaxial modulus function has a like effect on the computed shear function as shown in figure 3.7. However, this attempt at reconciling the measured and computed values does not account for the systematic difference of positive measurement error for the uniaxial data and negative systematic error for the shear measurements. Apart from this unresolved issue, it is clear by implication that accounting for potential measurement errors, even if they are not

[29] Although the rational for time-temperature shifting is questioned in this paper, we have included the Yee/Takemori data in a shifted form. See later for more discussion on this point.

identifiable unequivocally, could allow a reasonable correlation between measured and computed function values.

To address this systematic error in the computed functions, one possessing a positive and the other a negative value, one needs to consider the possibility that the bulk compliance contains a systematic error. One observes from equation (3.6) that this systematic error in the bulk compliance simultaneously affects the computations of E* and μ^* in opposite directions. Such computations were performed, with the result that the measured bulk compliance needs to be divided uniformly by a factor of 2.85 to effect a near agreement with the experimental data for E* and μ^*. The resulting computations are, nearly within plotting accuracy, equal to the dashed curves in figures 3.6 and 3.7 that were derived form multiplying the E* and μ^* data by a constant factor as discussed in the prior paragraph. Clearly, this factor on the bulk behavior is much too large to be accounted for by an error in the measurements of the bulk compliance. Here it is proper to recount that the dynamically measured bulk modulus agrees relatively closely with the value determined from wave propagation measurements at room temperature.

The situation with respect to the Poisson function is even less clear. While the measurements produce a monotonically declining function expected from general physical principles, the computations produced a virtually frequency (time) independent response. Moreover, that near-constant value, while intermediate to the function extremes, does not represent the average but is rather high for the range of frequencies considered.

To explore what functional dependence of the bulk response would be required to bring the computed and measured values into close agreement, the bulk compliance was –

again – multiplied by a uniform factor. It turns out that the magnitude of this factor affects only the (constant) value of the computed Poisson ratio, but does not influence the course of the function. The only way in which the functional variation of the Poisson Function could be addressed, so that the physically expected range of values follow, was to significantly change both the curvature and the amplitude of the bulk compliance function as indicated in figure 3.10. Clearly, the experimental bulk behavior did not allow for an error of the magnitude required to make such a large curvature change plausible, unless the whole time-temperature superposition principle were called into question.

A very important caveat needs to be raised here. Recall that the bulk related data derive mostly from measurements below the glass transition. The formation of the master-curves follows the rather widely practiced habit of the time-temperature superposition; while the temperature segments appear to "shift" rather well to form seemingly continuous master-curves for shear and uniaxial relaxation, one may question whether the practice is, in fact, justified. Superficially this observation may seem reasonable in view of the fact that the β-transition represents a complication for PMMA in the sub-T_g range. One could argue, however, that the linearized, phenomenological theory of viscoelasticity does not allow for such distinctions, as long as material functions are defined, and the properties displayed in figures 3.1 – 4 are reasonably smooth, with the Poisson function and the bulk compliance raising, perhaps, the greatest concern in this regard. While we cannot offer a definitive explanation for the discrepancies between measured and computed values, there is reasonable cause to investigate these issues on a, perhaps, broad basis that examines more carefully the time-temperature superposition, especially in the glassy domain.

Evidence that time-temperature shifting is not applicable, at least for PMMA, comes also more directly form the Yee/Takemori data. We show in figures 3.11 to 3.13, dynamic data derived from uniaxial deformation, but with the modulus and the Poisson function shifted while retaining the individual experimental points.[30] It is clear that the modulus and Poisson data contain curvatures that do not lend themselves unequivocally to shifting along the time axis without an arbitrary (temperature dependent) multiplication of the magnitudes. The strongest evidence that time-temperature shifting is inadmissible derives from the observation of the loss tangent for the uniaxial modulus, shown in figure 3.13: While this function is clearly "shiftable" for thermo-rheologically simple materials, these response segments at different temperatures do not fall into this category.

3.5 Concluding Remarks

A "complete" isotropic mechanical characterization of PMMA in terms of relaxation functions for uniaxial (tension) and shear behavior has been coupled with Poisson response under relaxation along with frequency dependent bulk compliance has been documented. All properties were determined on the same sample material, except the Poisson function. However, the uniaxial relaxation response of the two materials are, within experimental error, the same, so that one can be reasonably assured that the materials are virtually the same. Interconversion of the various material functions has been effected to compare computed with measured functions. Using the correspondence

[30] The data were digitized from enlarged scans of the figures in Yee and Takemori (1982). Moreover, the data shown in figures 3.11 and 3.12 have been "shifted" according to a slightly different shift mapping than the data represented in figures 3.6 and 3.9; in the latter figures the shifting has been accomplished to obtain a "best master-curve".

principle of the linearized theory of viscoelasticity in the frequency domain and with the use of the standard relations between the four measured material functions

a) the uniaxial response has been calculated from the shear and bulk properties,

b) the shear modulus from the uniaxial and bulk functions, and

c) the Poisson function from the shear and bulk properties and, finally,

d) an estimate (bounds) of the Poisson function from the uniaxial and bulk functions.

The differences between the computed and measured property functions are typically larger than measurement errors alone would allow. Results for a) and b) exhibit roughly constant disparity between computed and measured values, the computed uniaxial data being smaller than the measured one, and the computed shear modulus being larger than its experimental counterpart. To make both agree by allowing for a systematic error in the bulk compliance requires an unreasonably large change (error) in the bulk measurements, which is inconsistent not only with the accuracy of the current bulk compliance measurements but also with wave propagation results on the same material.

The computed Poisson function does not agree qualitatively with the measured (and expected) behavior, in that the computed values amount to essentially a constant value over a (temperature reduced) frequency range of about ten decades. Inordinately large differences in the bulk response would have to be postulated to bring the range of the computed and measured Poisson response into similarity. While the Poisson function measured by Yee and Takemori on a different PMMA material, is closer to the constant value computed here, it does indicate a measurable influence on frequency independent of

the fact that time-temperature shifting was used to enter that data into the frequency plot referenced to105 °C.

Inasmuch as the data under examination results from measurements below the glass transition temperature, it is deduced that the time-temperature shifting in that range needs to be re-examined, even though the data underlying the present developments seems to "shift" reasonably well to produce a master-curve – at least in the sense it is practiced in current material characterizations of polymers. The strongest support for this suggestion derives from data gathered on PMMA by Yee and Takemori, though that material is distinctly different from that studied here, which shows "non-shiftable" character in the time-temperature domain underlying their studies.

Finally we remark that if failure of the time-temperature shift principle is the cause for the lack of interconvertability of PMMA, then two possibilities offer themselves: One reason may be the presence of the β-transition in the glassy domain. In that event a more complicated analysis, accounting for the possible presence of two viscoelastic domains with different time-temperature behavior may have to be performed (Brinson and Knauss, 1991, 1992). The other reason may simply be that the principle, which is so well accepted and demonstrated in the rubbery domain for a large class of materials, is simply not applicable in the glassy region without significant modification(s). This question can be resolved only through performing studies over larger temperature and time domains than is typically exercised today. In particular, it would be advantageous to perform tests over time periods of months and years in addition to procuring short-term time-temperature segments for the construction of a master curve, provided physio-chemical stability can be assured.

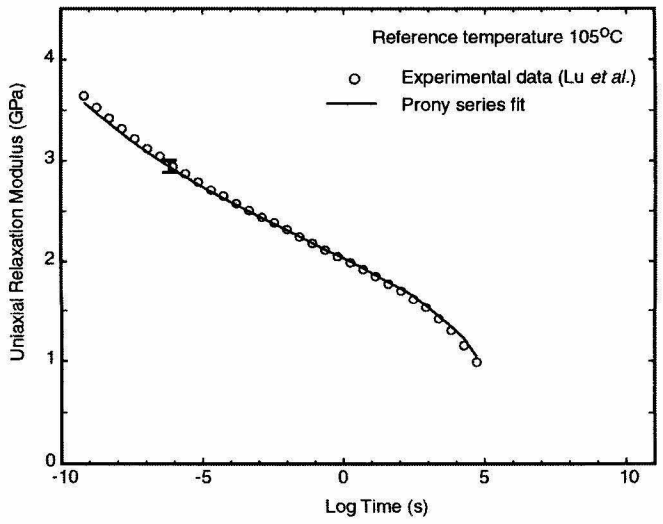

Figure 3.1: Master curve of uniaxial relaxation modulus at a reference temperature of 105 °C. A comparison of the prony series fit is also shown.

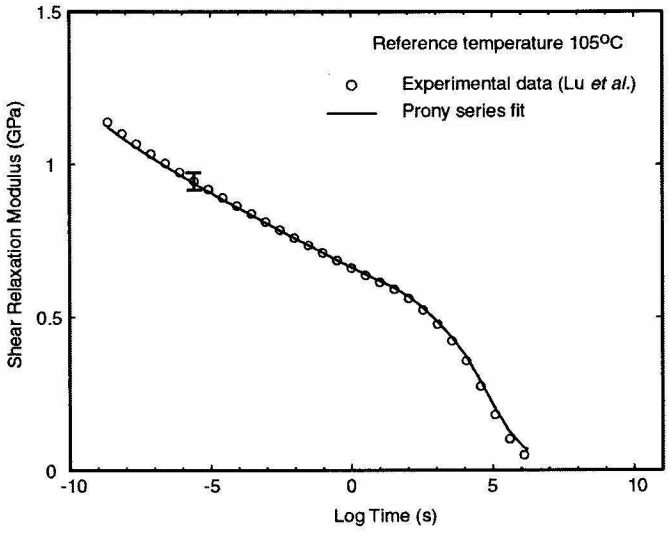

Figure 3.2: Master curve of shear relaxation modulus at a reference temperature of 105 °C. A comparison of the prony series fit is also shown.

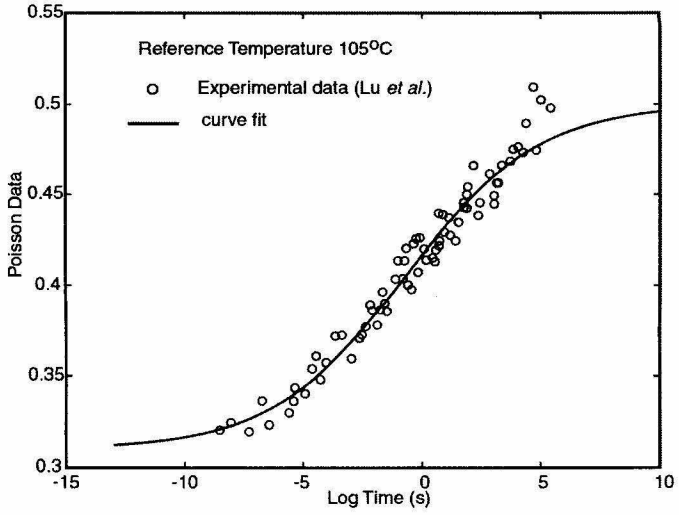

Figure 3.3: Master curve of Poisson's ratio at a reference temperature of 105 °C. Note the variations in the measured Poisson's data. The curve fitted to the data is also shown.

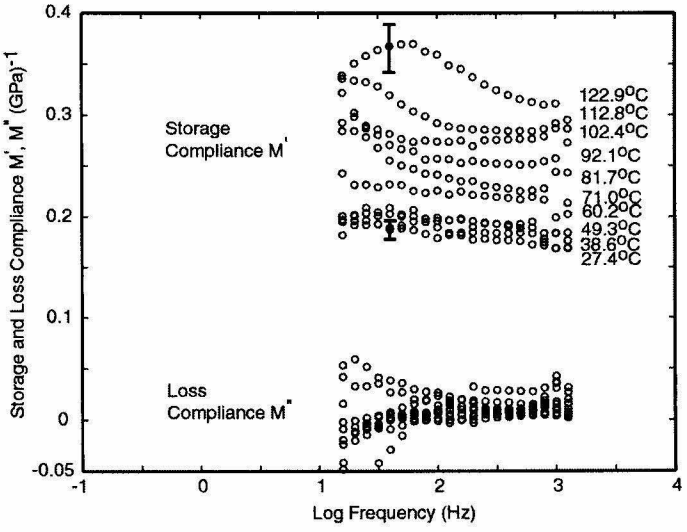

Figure 3.4: Storage M′ and loss compliance M″ of PMMA at indicated temperatures over two decades of frequency. Note error bar estimates at extreme temperatures.

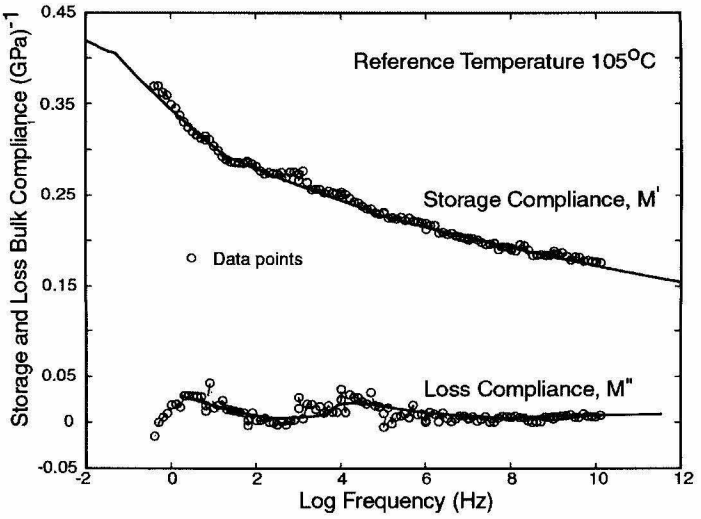

Figure 3.5: Master curves of storage and loss bulk compliances for PMMA at a reference temperature of 105 °C.

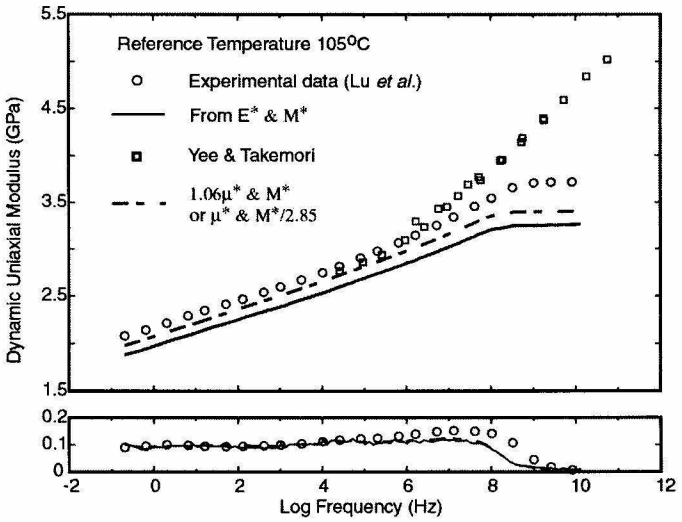

Figure 3.6: Comparison of dynamic uniaxial modulus, a) experimental data reported by Lu *et al.* (1997), b) computed data from dynamic shear modulus (Lu *et al.*, 1997) and dynamic bulk compliance (Sane and Knauss, 2000) measured on the same PMMA material. c) influence of uniform multiplicative factor: i) f = 1.06, applied to shear modulus data ii) f =1/2.85, applied to bulk compliance data and d) dynamic uniaxial modulus reported by Yee & Takemori (1982); data was shifted along the frequency axis by approximately six decades for the present reference temperature.

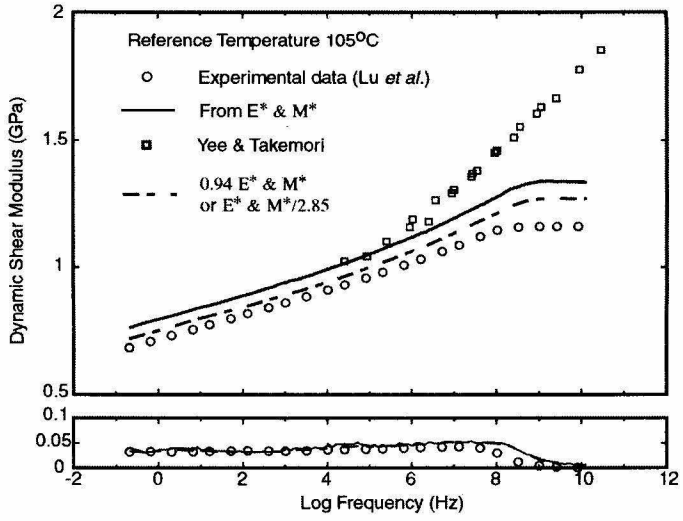

Figure 3.7: Comparison of dynamic shear modulus, a) experimental data reported by Lu *et al.* (1997), b) computed data from dynamic uniaxial modulus (Lu *et al.*, 1997) and dynamic bulk compliance (Sane and Knauss, 2000) measured on the same PMMA material. c) influence of uniform multiplicative factor: i) f = 0.94, applied to uniaxial modulus data ii) f =1/2.85, applied to bulk compliance data, and d) dynamic shear modulus reported by Yee & Takemori (1982); data was shifted along the frequency axis by approximately six decades for the present reference temperature.

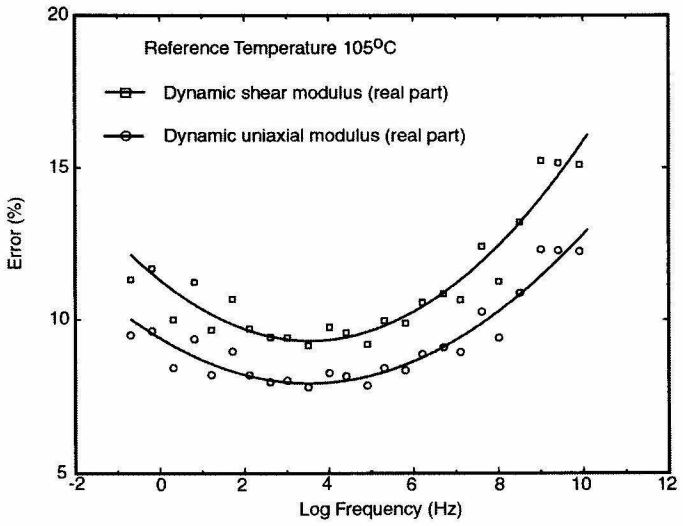

Figure 3.8: Error estimation between the measured and converted functions for dynamic uniaxial and shear modulus. The error calculations are based on the differences in storage modulus (real part) of the material functions.

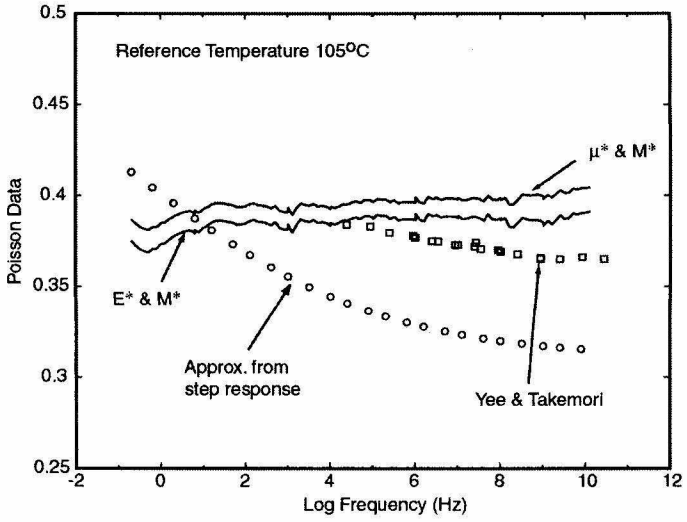

Figure 3.9: Comparison of Poisson data, a) computed data from dynamic shear modulus (Lu *et al.*, 1997) and dynamic bulk compliance (Sane and Knauss, 2000), b) computed data from dynamic uniaxial modulus (Lu *et al.*, 1997) and dynamic bulk compliance (Sane and Knauss, 2000), and c) approximate Poisson function derived from experimental data reported by Lu *et al.* (1997) under step response, d) dynamic Poisson's ratio reported by Yee & Takemori (1982); data was shifted along the frequency axis by approximately six decades for the present reference temperature.

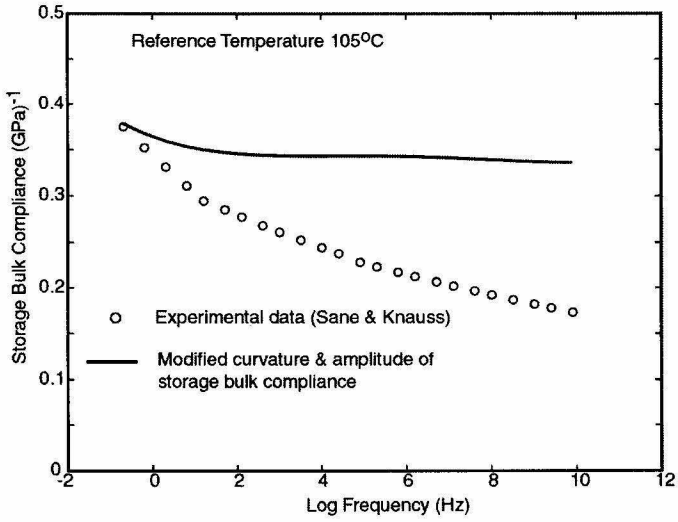

Figure 3.10: The modification in the curvature of the bulk compliance (real-part) required to account for the functional dependence of the computed Poisson's ratio with frequency.

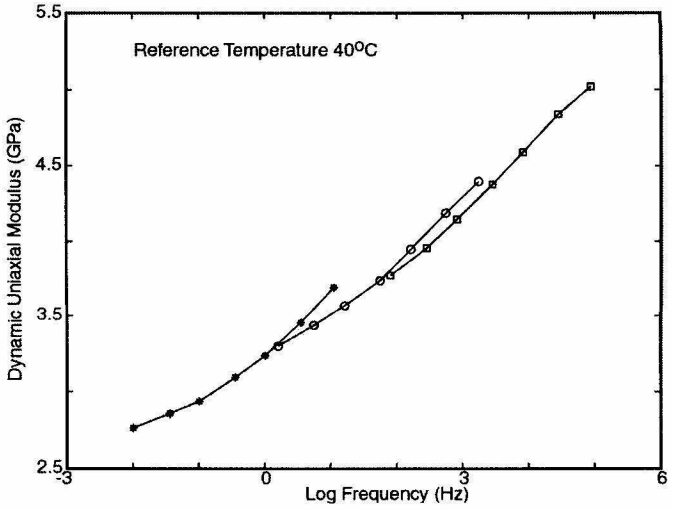

Figure 3.11: Master curve of uniaxial modulus, $|E^*|$ for PMMA at a reference temperature of 40 °C based on experimental data reported by Yee & Takemori (1982).

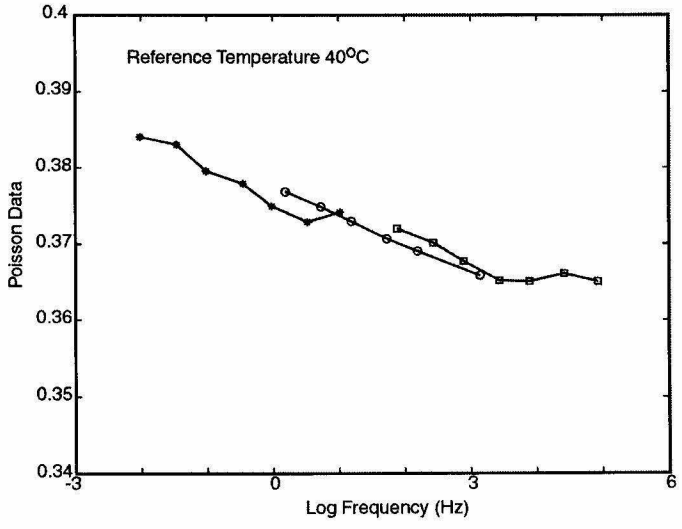

Figure 3.12: Master curve of Poisson's function, $|\nu^*|$ for PMMA at a reference temperature of 40 °C based on experimental data reported by Yee & Takemori (1982).

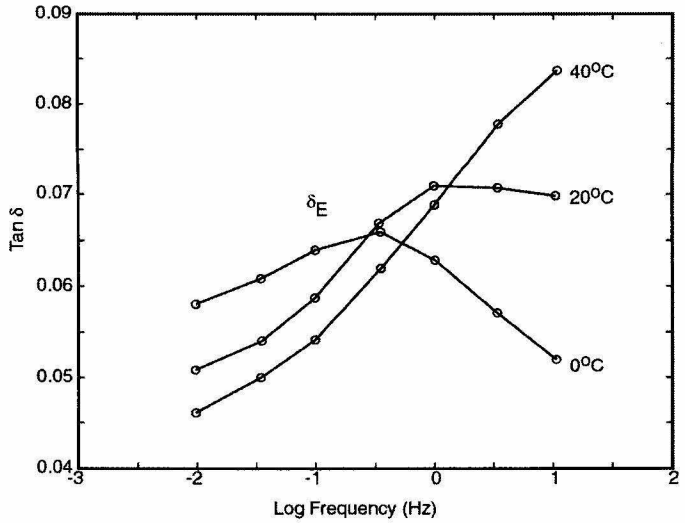

Figure 3.13: Loss tangent for the uniaxial modulus as reported by Yee & Takemori (1982).

Appendix A

In this section we present the details of the PVT and specific heat measurements on Di-2-ethylhexyl sebacate. The methods used for specific heat and PVT measurements were differential scanning calorimetry and high-pressure dilatometry respectively. The PVT measurements were carried over a pressure range of 10 to 200MPa and in a temperature range of 20° to 150 °C. The specific heat was determined as a function of temperature at atmospheric pressure. The oil sample was degassed for 12 hours under high vacuum. Tables A.1 and A.2 give the PVT and specific heat data. The values of specific heat at atmospheric pressure were extrapolated from the measured values at higher pressures. Table A.3 gives the values of the calculated adiabatic bulk compressibility of Di-2-ethylhexyl sebacate at atmospheric pressure. C-Mold Inc. carried out these measurements for us.

Table A.1: Pressure-volume-temperature data of Di-2-ethylhexyl sebacate at atmospheric pressure.

Temperature	Pressure, MPa				
°C	0	50	100	150	200
23	1.095	1.068	1.047	1.03	1.015
28	1.099	1.071	1.049	1.032	1.016
33	1.102	1.074	1.052	1.034	1.018
38	1.107	1.078	1.055	1.036	1.021
43	1.110	1.081	1.057	1.039	1.023
48	1.115	1.084	1.06	1.041	1.025
59	1.124	1.091	1.066	1.046	1.03
68	1.132	1.098	1.072	1.052	1.034
78	1.141	1.104	1.078	1.057	1.039
88	1.149	1.111	1.083	1.062	1.044
99	1.159	1.118	1.089	1.067	1.048
108	1.167	1.125	1.094	1.072	1.053
119	1.177	1.132	1.101	1.077	1.057
129	1.186	1.139	1.106	1.082	1.062
139	1.196	1.146	1.112	1.087	1.067
149	1.207	1.153	1.118	1.092	1.072

Table A.2: Variation of specific heat of Di-2-ethylhexyl sebacate at atmospheric pressure.

Temperature °C	Specific Heat J /Kg. °C
40	2075.86
50	2161.71
60	2202.88
70	2234.30
80	2274.27
90	2325.43
100	2349.02
110	2381.16
120	2415.11
130	2458.57
140	2501.18

Table A.3: Adiabatic bulk compressibility of Di-2-ethylhexyl sebacate at atmospheric pressure.

Temperature °C	Adiabatic Bulk Compressibility (GPa^{-1})
20	0.4678
30	0.4970
40	0.5278
50	0.5603
60	0.5946
70	0.6308
80	0.6689
90	0.7091
100	0.7515
110	0.7962
120	0.8432
130	0.8928
140	0.9450
150	1.0000

Similar measurements were carried out by Datapoint Testing Services[31] using the same methods and apparatus. However, in this case the oil sample was not degassed prior to carrying out the measurements in the (common) believe that pressurization dissolves gasses to insignificant levels in the liquid. However, upon comparing the two sets of PVT data (one obtained from C-Mold and other from Datapoint Testing Services), one observes a systematic difference between the specific volume at each pressure and temperature as demonstrated in figure A.1, which shows the variation of specific volume with temperature at different pressures. The adiabatic bulk compressibility (M_t) of the oil

[31] Datapoint Testing Services, 95 Brown Rd. #164, Ithaca, NY 14850

was calculated using the two sets of PVT data according to equation (1.3). As illustrated in figure A.2, the compressibility based on first PVT set agrees with the McKinney and Belcher data while similar calculations based on the second PVT set are approximately 20-25% higher. The adiabatic bulk compressibility, M_t, is a function of the specific volume (v), pressure (P), temperature (T) and specific heat (C_P). An error discussion for M_t is given below starting with the relative error

$$\left(\frac{\Delta M_t}{M_t}\right)^2 \cong 6\left(\frac{\Delta v}{v}\right)^2 + 4\left(\frac{\Delta \left.\frac{\partial v}{\partial T}\right|_P}{\left.\frac{\partial v}{\partial T}\right|_P}\right)^2 + \left(\frac{\Delta C_P}{C_P}\right)^2 \qquad \text{(A.1)}$$

where $\left.\frac{\partial v}{\partial T}\right|_P$ is the coefficient of thermal expansion.

In the two sets of PVT measurements, we observe a difference of approximately 5% between the specific volume and the coefficient of thermal expansion (represented by the slopes of the isobars) at atmospheric pressure. Using equation A.1 one finds that these differences are substantially amplified in the final values of the bulk compressibility, giving rise to a potential variation in the compressibility on the order on 20% at atmospheric pressure. Although these differences decrease with increasing pressure, the two sets of measurements are never in agreement with each other at any pressures. In view of the sensitivity of the bulk compressibility calculations, even a small error in the measurements of the specific volume is reflected significantly in the final compressibility values. For the two sets of measurements the methods and apparatus used for carrying out the PVT measurements were similar. The only perceived difference was that in the first case the oil was degassed while in the second case it was not. Thus from the differences

observed in the values of the bulk compressibility based on the two set of PVT data, one concludes that the presence of air, either in dissolved state or in the form of air bubbles, can alter the results significantly. However, the underlying assumption often made during such PVT measurements is that the air bubbles present in the oil would collapse under external pressures and the air is dissolved and that dissolved air will not effect the final values of the specific volume. Such measurements usually start from 10MPa upwards and values of specific volume at lower pressures are obtained through extrapolation. But the current measurement seems to contradict this underlying assumption.

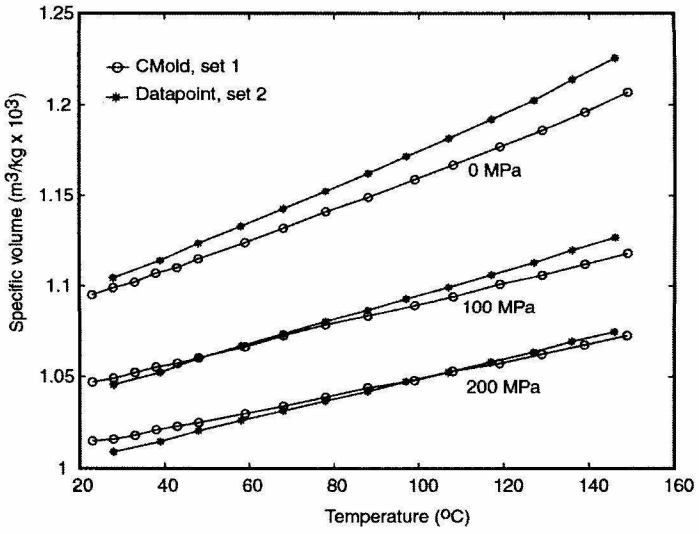

Figure A.1: Comparison between the PVT measurements for Di-2-ethylhexyl sebacate made by C-Mold Inc. and Datapoint Testing Services, at different pressures.

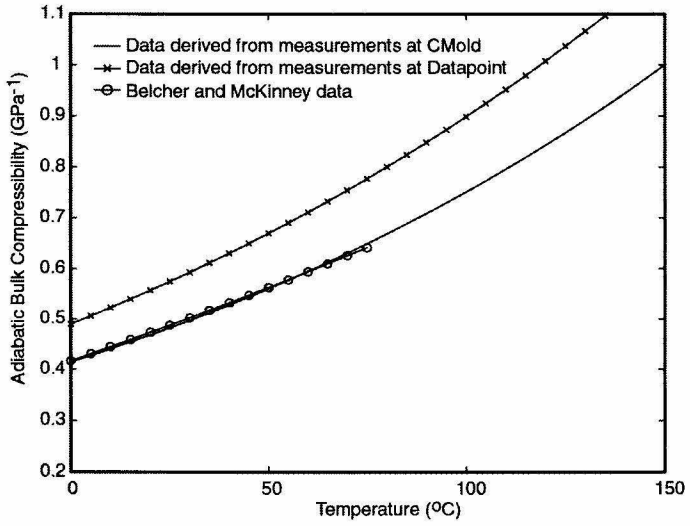

Figure A.2: Comparison of the adiabatic bulk compressibility of Di-2-ethyl hexyl sebacate: a) based on C-Mold measurements, b) based on Datapoint Services measurements, c) Belcher and McKinney data (obtained from J.E. McKinney via personal communication).

Appendix B

Here we present, for comparison purposes, the electrical feed-through employed by Deng and Knauss (1997). The assembly is diagrammed in figure B.1.

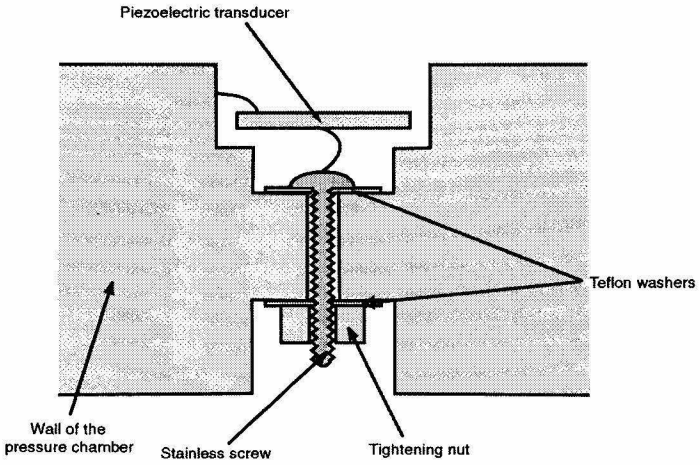

Figure B.1: Electrical feed-through; design used by Deng and Knauss (1997).

The feed-through consist of a screw-nut assembly and Teflon washers used for oil sealing and electrical insulation. The feed-through assembly was made by passing the screw through the small holes (1.78 mm in diameter) in both halves of the pressure chamber and tightening it with force just sufficient to form oil seal but not to damage the electrical insulation. The main disadvantage of this feed-through assembly was that the piezoelectric transducers had to be first soldered on to the screw and then carry out the assembly. This procedure was tedious and unreliable often leading to oil leaks or damage in the electrical insulation.

Appendix C

In this section we list in Tables C.1 and C.2 the dynamic bulk (storage and loss) compliance data obtained from measurements on PMMA specimen over a temperature range of 27° to 123 °C and over a frequency range of 10 to 1258 Hz.

Table C.1: Storage compliance of PMMA.

frequency Hz	Storage bulk compliance $(GPa)^{-1}$ with temperature (°C)									
	122.9	112.8	102.4	92.1	81.7	71.0	60.2	49.3	38.6	27.4
10.00	0.295	0.319	0.289	0.336	0.332	0.225	0.199	0.202	0.198	0.191
12.59	0.316	0.312	0.353	0.346	0.312	0.239	0.170	0.147	0.156	0.186
15.85	0.339	0.336	0.285	0.293	0.322	0.243	0.201	0.197	0.182	0.195
19.95	0.351	0.334	0.299	0.303	0.284	0.232	0.202	0.201	0.196	0.192
25.12	0.358	0.333	0.290	0.287	0.278	0.232	0.209	0.204	0.197	0.192
31.62	0.364	0.328	0.286	0.281	0.268	0.229	0.205	0.201	0.193	0.193
39.81	0.367	0.320	0.282	0.271	0.255	0.232	0.209	0.203	0.189	0.187
50.12	0.369	0.311	0.277	0.267	0.250	0.231	0.203	0.201	0.192	0.189
63.10	0.370	0.304	0.274	0.264	0.247	0.225	0.207	0.201	0.196	0.187
79.43	0.362	0.299	0.275	0.256	0.243	0.224	0.199	0.198	0.195	0.183
100.00	0.359	0.292	0.274	0.257	0.241	0.226	0.199	0.196	0.190	0.179
125.89	0.349	0.289	0.274	0.257	0.238	0.222	0.197	0.196	0.184	0.182
158.49	0.345	0.287	0.275	0.253	0.235	0.225	0.198	0.197	0.184	0.182
199.53	0.337	0.286	0.269	0.255	0.235	0.221	0.196	0.190	0.185	0.177
251.19	0.330	0.286	0.275	0.253	0.231	0.221	0.194	0.193	0.184	0.178
316.23	0.324	0.285	0.276	0.252	0.229	0.219	0.193	0.193	0.184	0.177
398.11	0.320	0.284	0.276	0.252	0.228	0.219	0.192	0.190	0.183	0.177
501.19	0.316	0.284	0.277	0.251	0.225	0.217	0.193	0.189	0.184	0.176
630.96	0.313	0.284	0.276	0.252	0.226	0.219	0.195	0.189	0.184	0.172
794.33	0.310	0.286	0.279	0.254	0.228	0.217	0.178	0.184	0.175	0.171
1000.00	0.311	0.292	0.287	0.257	0.244	0.199	0.183	0.184	0.169	0.169
1258.93	0.295	0.286	0.273	0.243	0.213	0.202	0.176	0.184	0.169	0.169

Table C.2: Loss compliance of PMMA.

frequency Hz	Loss bulk compliance $(GPa)^{-1}$ with temperature (°C)									
	122.9	112.8	102.4	92.1	81.7	71.0	60.2	49.3	38.6	27.4
10.00	-0.134	-0.085	-0.055	-0.002	0.040	-0.030	-0.037	-0.029	-0.013	-0.005
12.59	-0.142	-0.044	-0.025	0.023	0.082	-0.033	0.000	-0.053	-0.008	0.003
15.85	-0.095	-0.048	-0.019	0.042	0.053	-0.009	-0.002	-0.042	-0.024	0.016
19.95	-0.078	-0.020	-0.013	0.033	0.059	-0.011	-0.012	-0.012	-0.007	-0.001
25.12	-0.059	-0.009	-0.006	0.033	0.052	-0.003	-0.014	-0.007	-0.004	0.002
31.62	-0.042	0.003	-0.004	0.036	0.041	-0.007	-0.006	-0.008	0.004	0.003
39.81	-0.029	0.005	0.002	0.027	0.039	0.002	-0.009	0.000	0.001	0.008
50.12	-0.015	0.012	0.002	0.027	0.036	-0.005	0.002	0.005	0.006	0.004
63.10	0.000	0.015	0.004	0.020	0.030	-0.001	0.009	0.001	0.005	0.007
79.43	0.006	0.019	0.000	0.020	0.028	0.006	0.001	0.003	0.005	0.007
100.00	0.010	0.024	-0.001	0.014	0.027	0.007	0.010	0.006	0.002	0.009
125.89	0.019	0.014	-0.003	0.017	0.023	0.010	0.004	0.000	0.000	0.006
158.49	0.020	0.013	0.000	0.010	0.020	0.005	0.001	0.000	0.000	0.005
199.53	0.017	0.012	-0.003	0.018	0.033	0.019	0.004	0.005	0.000	0.010
251.19	0.029	0.011	0.001	0.011	0.018	0.008	0.007	0.007	0.006	0.007
316.23	0.029	0.010	0.003	0.011	0.017	0.009	0.007	0.006	0.005	0.006
398.11	0.029	0.010	0.003	0.011	0.017	0.010	0.007	0.009	0.005	0.006
501.19	0.028	0.010	0.004	0.011	0.016	0.011	0.006	0.007	0.006	0.008
630.96	0.028	0.011	0.004	0.009	0.015	0.013	0.010	0.009	0.009	0.006
794.33	0.031	0.012	0.006	0.012	0.016	0.023	0.019	0.007	0.015	0.005
1000.00	0.043	0.015	0.011	0.031	0.036	0.037	0.018	0.010	0.006	0.004
1258.93	0.032	0.016	0.016	0.020	0.027	0.011	0.007	0.004	0.007	0.002

Appendix D

Here we list the forms of energy expressions used in the Dreiding force field. All parameters in the equations can be found in Dreiding's paper (Mayo *et al.*, 1990).

Bond interactions:

$$E_B = \frac{1}{2} k_e (R - R_e)^2 \qquad E_T = \frac{1}{2} V \{1 - \cos[n (\varphi - \varphi_o)]\}$$

$$E_A = \frac{1}{2} K (\theta - \theta_o)^2 \qquad E_I = \frac{1}{2} K_{inv} (\Psi - \Psi_o)^2$$

Non-bonded interactions:

$$E_{vdw} = D_0 \left\{ \left[\left(\frac{6}{\zeta - 6} \right) \exp^{\zeta (1 - (R/R_o))} \right] - \left[\left(\frac{\zeta}{\zeta - 6} \right) \left(\frac{R_o}{R} \right)^6 \right] \right\}$$

$$E_{coul} = C_0 \sum_i \sum_{j>i} \frac{Q_i Q_j}{\varepsilon R_{ij}}$$

Appendix E

Prediction of the glass transition temperatures of amorphous polymers using molecular dynamics simulations has evoked considerable interest. One of the most straightforward experimental methods for characterizing the glass transition temperature is by measuring volume (or density) as a function of temperature. In principle, this process can be simulated on a computer by performing NPT dynamics to evaluate equilibrium volume at a constant temperature. In this section we describe briefly our attempts to determine the glass transition temperature of the amorphous PMMA using molecular dynamics simulations. We realize that the current studies are by no means complete and the results presented here bear preliminary character.

The NPT dynamics simulation was carried out on one of the samples of PMMA at atmospheric pressure and over a temperature range of zero to 700 K. The same parameters as described in Section 2.3 were used during these calculations. Initially, 25 ps MD simulations were executed over a temperature range of zero to 700 K, in which the temperature was increased in steps of 100 K. The PMMA sample was then "cooled" from 700 K to 100 K by performing 15 ps MD simulations run for each temperature during which the temperature was decreased in steps of 50 K over a temperature range of 500 to 200 K. The final values of density were computed through averaging as mentioned in Section 2.3.

In figure E.1 the variation of the density with temperature is plotted at atmospheric pressure. The uncertainties are estimated by comparing the density values obtained during the heating-and-cooling cycle and were found to increase to 2-3% for temperatures beyond 350 K as the fluctuations in the density data increased with temperatures. From

figure E.1, one can clearly identify two distinct regions, namely, a "glassy domain" ("low" temperatures) and a "rubbery domain" ("high" temperatures). Linear curves were fitted through the density data in these regions and the temperature at which the two curves intersected was considered as the glass transition temperature. In this manner the glass transition temperature was estimated to be 420 K (± 50 K) which is higher than the experimentally observed value of 378 K for amorphous PMMA. The estimation of the uncertainty in the computed glass transition temperature was based on the uncertainties in the density data.

Although the prediction of glass transition temperature is not very accurate, the results are certainly encouraging. The current simulations were carried out on only one PMMA sample and over a shorter time period (15 ps) with much larger temperature increments (50 K) in comparison to some of the other investigations on glass transition (Fan *et al.*, 1997 on polycarbonate; Soldera, 1998, on PMMA) in which simulations were performed over much longer time periods (100 ps) and the temperature increments were limited to less than 20 K near glass transition. Because of the relatively large temperature increments and fluctuations in the density data, it was difficult to pinpoint the glass transition temperature accurately. To increase the precision of the predictions, it is essential to perform more simulations between a temperature range of 350 to 450 K over longer time duration with much small temperature increments.

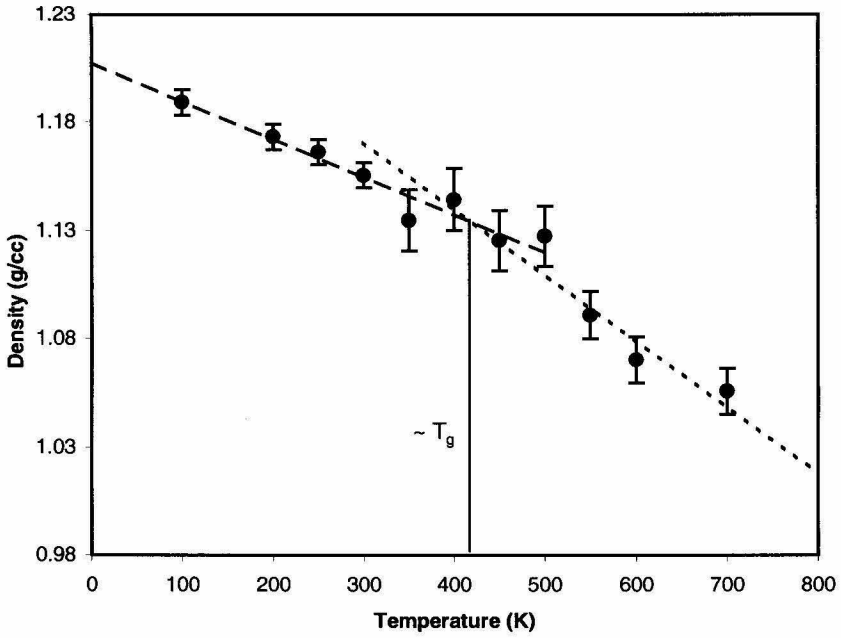

Figure E.1: Prediction of glass transition temperature of amorphous PMMA using molecular dynamics simulations.

References

Andersen, H. C., "Molecular Dynamics Simulations at Constant Pressure and/or Temperature," J. Phys. Chem., **72**, 1980, 2384.

Brandrup, J. and Immergut, E.H., "Polymer Handbook," Wiley, New York, 1989.

Brinson, L.C. and Knauss, W.G., "Thermorheologically Complex Behavior of Multi-Phase Viscoelastic Materials," J. Mechanics and Physics of Solids **39**, 1991, 859.

Brinson, L.C. and Knauss, W.G., "Finite Element Analysis of Multi-Phase Viscoelastic Solids," J. Applied Mechanics **59**, 1992, 730.

Deng, T.H., "Measurements of Dynamic Bulk Compliance of Polymers," Ph.D. thesis, California Institute of Technology, Pasadena, 1997.

Deng, T.H. and Knauss, W.G., "The Temperature and Frequency Dependence of the Bulk Compliance of Poly (Vinyl Acetate). A Re-Examination," Mechanics of Time-Dependent Materials **1,** 1997, 33.

Deutsch, K., Hoff, E.A.W., and Reddish, W., J. Polymer Sci. **13**, 1954, 565.

Duran, R.S. and McKenna, G.B., "A Torsional Dilatometer for Volume Change Measurements on Deformed Glasses: Instrument Description and Measurements on Equilibrated Glasses," J. Rheology, **34**, 1990, 813.

Emri, I. and Tschoegl, N.W., "Generating Line Spectra from Experimental Responses. Part I: Relaxation Modulus and Creep Compliance," Rheol. Acta **32**, 1993, 311.

Emri, I. and Tschoegl, N.W., "Generating Line Spectra from Experimental Responses. 4. Application to Experimental-Data," Rheol. Acta **33**, 1994, 60.

Evans, D.J. and Morriss, G.P., "Statistical Mechanics of Nonequilibrium Liquids," Academic Press Limited, 1990.

Fan, C. F., Cağin, T., and Chen, Z.M., "Molecular Modeling of Polycarbonate. 1. Force Field, Static Structure, and Mechanical Properties," Macromolecules, **27**, 1994, 2383.

Fan, C. F., Cağin, T., Shi, W., and Smith, K.A., "Local Chain Dynamics of a Model Polycarbonate Near Glass Transition Temperature: A Molecular Dynamics Simulation," Macromol. Theory Simul., **6**, 1997, 83.

Fan, C.F. and Hsu, S.L., "Application of the Molecular Simulation Technique to Characterize the Structure and Properties of an Aromatic Polysulfone System. 2. Mechanical and Thermal Properties," Macromolecules, **25**, 1992, 266.

Ferry, J.D., Child, W.C. Jr., Zand, R., Stern, D.M., Williams, M.L., and Landel, R.F., "Dynamical Mechanical Properties of Poly (Ethyl Methacrylate)," J. Colloid Science **12**, 1957, 53.

Gao, J. and Weiner, J.H., "Bond Orientation Decay and Stress Relaxation in a Model Polymer Melt," Macromolecules, **29**, 1996, 6048.

Haile, J. M.," Molecular Dynamics Simulation," John Wiley & Sons, 1997.

Heydemann, P., "The Dynamic Compressibility of High Polymers in the Frequency Range from 0.1 c/s to 60 kc/s," Acustica **9**, 1959, 446.

Heymans, L.J., "An Engineering Analysis of Polymer Film Adhesion to Rigid Substrates," Ph.D. thesis, California Institute of Technology, Pasadena, 1983.

Hoover, W. H., "Canonical Dynamics: Equilibrium Phase-Space Distributions," Phys. Rev. A, **31**, 1985, 1695.

Iwayanagi, S. and Hideshima, T., "Low Frequency Coupled Oscillator and its Application to High Polymer Study," J. Phys. Soc. Jpn. **8**, 1953, 365.

Karawasa, N. and Goddard, W.A., "Acceleration of Convergence for Lattice Sums," J. Phys. Chem., **93**, 1989 7320.

Karawasa, N. and Goddard, W.A., "Dielectric Properties of Poly(vinylidene fluoride) from Molecular Dynamics Simulations," Macromolecules, **28**, 1995, 6765.

Kästner, S. and Pohl, G., "Ein Beitrag zur Frage der vollständigen Erfassung des Mechanischen Relaxationsverhaltens der Polymeren," Kolloid Z. Z. Polym. **191**, 1963, 114.

Khare, R., de Pablo, J.J., and Yethiraj, A., "Rheology of Confined Polymer Melts," Macromolecules, **29**, 1996, 7910.

Knauss, W.G. and Emri, I.J., "Non-Linear Viscoelasticity based on Free Volume Consideration," Computers and Structures, **13**, 1981, 123.

Knauss, W.G. and Emri, I.J., "Volume Change and the Non-Linearly Thermo-Viscoelastic Constitution of Polymers," Polymer Engineering and Science, **27**, 1987, 86.

Knauss, W.G. and Kenner, V.H., "On the Hydrothermomechanical Characterization of Poly Vinyl Acetate," J. Appl. Phys. **51**, 1980, 5131.

Kono, R., "The Dynamic Bulk Viscosity of Polystyrene and Poly (Methyl Methacrylate)," J. Phys. Soc. Jpn. **15**, 1960, 718.

Kubát, J., "Stress Relaxation in Solids," Nature, **204**, 1963, 378.

Kubát, J. and Rigdhal, M., "The Exponential and Power Laws of Stress Relaxation Kinetics and a General Relation between the Activation Volume and Effective Stress," Phys. Stat. Sol., (a) **35**, 1976, 173.

Kubát, J. and Rigdhal, M., "Stress-Relaxation Behavior of Solid Polymers," in Failure of Plastics, W. Brostow and R.D. Corneliussen (eds.), Hanser New York, 1986, 60.

Kusanagi, H., Chatani, Y., and Tadokoro, H., "The Crystal Structure of Isotactic Poly (Methyl Methacrylate): Packing-Mode of Double Stranded Helices," Polymer, **35**, 1994, 2028.

Lee, S.H. and Cummings, P.T., "The Rheology of n-Decane and 4-Propyl heptane by Non-equilibrium Molecular Dynamics Simulations," Mol. Simulat, **21(1)**, 1998, 27.

Lin, T.S. and Nolle, A.W., " Dynamic Compressibility of Poly (Vinyl Acetate) and Poly (Methyl Methacrylate): Effects of Molecular Weight," Polymer **30**, 1989, 648.

Losi, G.U. and Knauss, W.G., "Free Volume Theory and Nonlinear Thermoviscoelasticity," Polymer Science and Engineering, **32**, 1992, 542.

Lu, H., "Nonlinear Thermo-Mechanical Behavior of Polymers under Multiaxial Loading," Ph.D. thesis, California Institute of Technology, Pasadena, 1997.

Lu, H. and Knauss, W.G., "Non-Linear Viscoelastic Behavior of PMMA under Multiaxial Stress States," Mech. Time-Dep. Mat., **1**, 1997.

Lu, H., Zhang, X., and Knauss, W.G., "Uniaxial, Shear, and Poisson Relaxation and Their Conversion to Bulk Relaxation: Studies on Poly (Methyl Methacrylate)," J. Polymer Engineering and Science **37**, 1997, 1.

Ma, Z. and Ravi-Chandar, K., "Confined Compression: A Stable Homogeneous Deformation for Constitutive Characterization," Experimental Mechanics **40**, 2000, 38.

Mayo, S. L., Olafson, B. D., and Goddard, W. A., "Dreiding – A Generic Force-Field for Molecular Simulations ," J. Phys. Chem., **94**, 1990, 8897.

McKinney, J.E. and Belcher, H.V., "Dynamic Compressibility of Poly (Vinyl Acetate) and its Relation to Free Volume," J. Research of National Bureau of Standards, A. Physic and Chemistry **67A**, 1963, 43.

McKinney, J.E., Edelman, S., and Marvin, R.S., "Apparatus for the Direct Determination of the Dynamic Bulk Modulus," J. Appl. Phys. **27**, 1956, 425.

McKinney, J.E. and Goldstein, M.J., "PVT Relationships for Liquid and Glassy Poly (Vinyl Acetate)," J. Research of National Bureau of Standards, A. Physic and Chemistry **78A**, 1974, 331.

McCrum, N.G., Read, B.E., and Williams, G., "Anelastic and Dielectric Effects in Polymeric Solids," Wiley, London, 1967.

Parrinello, M. and Rahman, A., "Crystal Structure and Pair Potentials: A Molecular-Dynamics Study," Phys. Rev. Lett., **45**, 1980, 1196.

Parrinello, M. and Rahman, A., "Polymorphic Transitions in Single Crystals: A New Molecular Dynamics Method," J. Appl. Phys., **52**, 1981, 7182.

Parrinello, M. and Rahman, A., "Strain Fluctuations and Elastic Constants," J. Phys. Chem., **76**, 1982, 2662.

Rappé, A. W., Casewit, C. J., Colwell, K. S., Goddard, W. A., and Skiff, W. M.," UFF, A Full Periodic-Table Force-Field for Molecular Mechanics and Molecular-Dynamics Simulations," J. Am. Chem. Soc., **114**, 1992, 10024.

Rappé, A. W. and Goddard, W. A., "Charge Equilibration for Molecular-Dynamics Simulations," J. Phys. Chem., **95**, 1991, 3358.

Sane, S.B., Cağin, T., and Knauss, W.G., "MD Simulations of Amorphous PMMA to Compute Bulk Compliance as a Function of Temperature," in preparation.

Sane, S.B. and Knauss, W.G.,"The Time-Dependent Bulk Response of Poly (Methyl-Methacrylate) (PMMA)," in preparation.

Sarman, S.S., Evans, D.J., and Cummings, P.T., "Recent Developments in Non-Newtonian Molecular Dynamics," Physics Reports, **305**, 1998, 1.

Schapery, R.A., "Approximate Methods of Transform Inversion for Viscoelastic Stress Analysis," Proceedings of the fourth U.S. National Congress on Applied Mechanics, ASME, 1075.

Soldera, A., "Comparison Between the Glass Transition Temperatures of the Two PMMA Tacticities: A Molecular Dynamics Simulation Point of View," Macromol. Symp., **133**, 1998, 21.

Sun, H, "COMPASS: An Ab Initio Force-Field Optimized for Condensed-Phase Applications - Overview with Details on Alkane and Benzene Compounds," J. Phys. Chem. B, **102** (38), 1998, 7338.

Thompson, P.A., "Compressible-Fluid Dynamics," McGraw-Hill, New York, 1972.

Tschoegl, N.W., "The Phenomenological Theory of Linear Viscoelastic Behavior," Springer-Verlag, New York, 1989.

Wada, Y., Hirose, H., Umebayashi, H., and Otomo, M., J. Phys. Soc. Jpn. 15, 1960, 2324.

Yee, A.F. and Takemori, M.T., "Dynamic Bulk and Shear Relaxation in Glassy Polymers. I. Experimental Techniques and Results on PMMA," J. Polymer Science, **20**, 1982, 205.